OBSAH

ÚVODNÍ SLOVO 2
Rostislav Drochytka

WTA V ČESKÉ REPUBLICE / Pracovní skupiny 4

HOLLOWED HERITAGE – DETERIORATION OF DOBŘÍŠ HISTORIC STONE BRIDGE AFTER INCOMPATIBLE REPAIR 5
OHROŽENÉ HISTORICKÉ DĚDICTVÍ – DEGRADACE HISTORICKÉHO KAMENNÉHO MOSTU V DOBŘÍŠI V DŮSLEDKU POUŽITÍ NEVHODNÝCH OPRAVNÝCH MATERIÁLŮ
BAUEROVÁ Pavla1, FRANKEOVÁ Dita, NÁHUNKOVÁ Pavla, SLÍŽKOVÁ Zuzana

FINITE ELEMENT ASSESSMENT OF A COMPOSITE ROOF WATERPROOFING SYSTEM UNDER COMBINED 11
ENVIRONMENTAL LOADING
POSOUZENÍ KOMPOZITNÍHO STŘEŠNÍHO HYDROIZOLAČNÍHO SYSTÉMU METODOU KONEČNÝCH PRVKŮ PŘI KOMBINOVANÉM PŮSOBENÍ VLIVŮ PROSTŘEDÍ
Narges Azadvar, William Jack Finley, Maurizio Guadagnini, Iman Hajirasouliha

NOVÝ BETON VE STARÉM ZDIVU? Z DĚJIN INOVACÍ. 18
NEW CONCRETE IN OLD MASONRY? FROM THE HISTORY OF INNOVATIONS.
Mgr. Lukáš Beran, Ph.D.

DECONTAMINATION AND CLEANING OF INTERIOR NATURAL STONE SURFACES AT NOTRE-DAME 22
DE PARIS AFTER THE 2019 FIRE
DEKONTAMINACE A ČIŠTĚNÍ VNITŘNÍCH POVRCHŮ Z PŘÍRODNÍHO KAMENE V KATEDRÁLE NOTRE-DAME V PAŘÍŽI PO POŽÁRU V ROCE 2019
Dipl.-Ing. Jens Engel

THERMAL COMPATIBILITY OF REPAIR MORTARS WITH STONE AND BRICK SUBSTRATES. 27
HODNOCENÍ TEPLOTNÍ KOMPATIBILITY OPRAVNÝCH MALT S KAMENNÝM A CIHELNÝM PODKLADEM
NÁHUNKOVÁ Pavla, FRANKEOVÁ Dita, MÁCOVÁ Petra and KUNECKÝ Jiří

MECHANICAL AND CHROMATIC RESPONSE OF COARSE-GRAINED SANDSTONE SUBJECTED TO ELEVATED 31
TEMPERATURES
ZMĚNY MECHANICKÝCH VLASTNOSTÍ A BARVY HRUBOZRNNÉHO PÍSKOVCE VLIVEM VYSOKÝCH TEPLOT
Ema Jankovičová and Radek Zigler

CATHODIC PROTECTION AS AN INNOVATIVE REHABILITATION TECHNIQUE WITH CASE STUDIES FROM GERMANY . 36
KATODICKÁ OCHRANA JAKO INOVATIVNÍ SANAČNÍ METODA S PŘÍPADOVÝMI STUDIEMI Z NĚMECKA
Hernâni Esteves, Andreas Tobler

Zpravodaj WTA CZ

Vydavatel: Vědeckotechnická společnost pro sanace staveb a péči o památky z.s. (WTA CZ),
Novotného lávka 5, 116 68 Praha 1, IČO: 75088762, tel.: 221 082 397, e-mail: wta@wta.cz, www.wta.cz

Vychází: 2 až 4x ročně Číslo vychází: 12. 11. 2026

Redakční rada / Editorial Board: Ing. Lenka Mészárosová, Ph.D. (šéfredaktor), Ing. Radka Navrátilová, Ph.D. (zástupce šéfredaktora), prof. Ing. Rostislav Drochytka, CSc., MBA, dr. h. c., Ing. arch. Karel Doubner, prof. Dr.-Ing. Harald Garrecht, prof. Dr.-Ing. Rolf P. Gieler, CSc., prof. dr hab. inż. Jacek Śliwiński, doc. Ing. Jan Vaněrek, Ph.D., Prof. Dr. Alexandra Troi, Dipl.-Ing. Dr. Clemens Hecht, Dipl.-Ing. Gero Hebeisen, dr inż. Bartłomiej Monczyński, doc. Ing. Vít Černý, Ph.D.

Litografie a tisk: Expressprint

Registrace povolena na Ministerstvu kultury ČR pod číslem MK ČR E 13411, ISSN 1213-7308 (Print), ISSN 2788-3264 (On-line)
Za obsah a původnost článků odpovídají jejich autoři. Odborné články byly recenzovány. Názory v příspěvcích se nemusejí shodovat s názory redakce.
The authors are responsible for the content and originality of the contributions. The contributions were reviewed. The opinions of editors can be inconsistent with those of the authors.

ÚVODNÍ SLOVO

Vážené kolegyně, vážení kolegové,

dovolte mi, abych Vás srdečně pozdravil u příležitosti konání 48. konference Sanace a rekonstrukce staveb a 28. mezinárodní konference CRRB – Conference on Rehabilitation and Reconstruction of Buildings, které se konají ve dnech 12.–13. listopadu 2026 na Fakultě stavební Vysokého učení technického v Brně. Tradiční setkání pořádá WTA CZ ve spolupráci s Fakultou stavební VUT v Brně a nabízí příležitost sdílet nové poznatky i zkušenosti z konkrétních realizací. Velký dík celému organizačnímu týmu, zejména Ing. Lence Mészárosové, Ph.D., Ing. Jindřichu Melicharovi, Ph.D. a Ing. Peti Lacikové.

Konference tradičně dlouhodobě propojuje výzkumné pracovníky s projektanty, diagnostiky, zástupci realizačních firem a odborníky v oblasti památkové péče. Letošní tematické zaměření zahrnuje sanace zdiva a betonových konstrukcí, ochranu dřeva, povrchové technologie, přírodní i umělý kámen, stavební fyziku, statiku a požární ochranu. Mezinárodní část CRRB rozšiřuje prostor pro porovnání přístupů k obnově staveb a pro navázání spolupráce se zahraničními kolegy.

Za podstatné považuji zejména propojení kvalitní diagnostiky s návrhem sanačního zásahu a následným ověřením jeho účinnosti. Při obnově staveb hledáme řešení, která prodlužují jejich životnost, respektují vlastnosti původních materiálů a umožňují hospodárné využívání existujících konstrukcí. Právě otevřená diskuse nad výsledky výzkumu a zkušenostmi z praxe nám pomáhá posuzovat vhodnost jednotlivých postupů.

Na mezinárodní úrovni pokračuje WTA International v přípravě a aktualizaci odborných směrnic. Mezi letošní novinky patří vydaná směrnice 3-20 pro sanaci historického cihelného zdiva a nové dokumenty řady 11 věnované požární ochraně stávajících a památkových staveb, konkrétně zvláštním stavbám a klasifikaci stávajících stavebních prvků. K odbornému připomínkování jsou zveřejněny také návrhy dokumentů zaměřených na sanační omítkové systémy, výskyt plísní na dřevě, radon ve stávajících budovách a průzkum a hodnocení vlastností zdiva. Pro naši odbornou komunitu představují příležitost zapojit do mezinárodní diskuse také české zkušenosti.

Významnou součástí činnosti WTA zůstává podpora nastupující generace odborníků. Vedle české soutěže o nejlepší diplomové a disertační práce nabízí mladým odborníkům možnost mezinárodního uplatnění také ocenění WTA Young Professionals Award. V roce 2026 bylo poprvé uděleno také v kategorii Practical, což vítám jako ocenění kvalitní praktické práce. Přihlášky do ročníku 2027 je možné podávat do 30. listopadu 2026.

Rád bych Vás současně pozval na mimořádné setkání WTA-Tage 2027 „50 let WTA“, které se uskuteční ve dnech 18.–20. března 2027 v Mnichově. WTA si připomíná padesát let od svého vzniku v roce 1976 a jubilejní oslavy vyvrcholí právě tímto březnovým setkáním. Slavnostní oslava je plánována na 18. března na zámku Nymphenburg. Součástí programu budou rovněž valná hromada WTA International, odborné kolokvium a závěrečná exkurze. Věřím, že se zde setkáme v početném českém zastoupení a společně si připomeneme význam mezinárodní spolupráce pro sanace staveb a péči o památky.

Závěrem děkuji všem členům WTA CZ, autorům příspěvků, organizátorům a partnerům za jejich práci a dlouhodobou podporu. Přeji Vám inspirativní konferenční jednání, přínosné diskuse a příjemná osobní setkání v Brně. Těším se na naši další spolupráci.

prof. Ing. Rostislav Drochytka, CSc., MBA, dr. h. c.
předseda WTA CZ

INTRODUCTORY WORD

Dear Colleagues,

It is my great pleasure to welcome you on the occasion of the 48th Conference on Building Rehabilitation and Reconstruction and the 28th International Conference CRRB – Conference on Rehabilitation and Reconstruction of Buildings, which take place on 12–13 November 2026 at the Faculty of Civil Engineering, Brno University of Technology. This traditional event is organised by WTA CZ in cooperation with the Faculty of Civil Engineering of Brno University of Technology and provides an opportunity to share new findings and practical experience gained from specific projects. My sincere thanks go to the entire organising team, especially to Ing. Lenka Mészárosová, Ph.D., Ing. Jindřich Melichar, Ph.D., and Ing. Petra Laciková.

For many years, this conference has traditionally brought together researchers, designers, building diagnostics specialists, representatives of construction companies and experts in heritage conservation. This year's thematic scope covers the rehabilitation of masonry and concrete structures, timber protection, surface technologies, natural and artificial stone, building physics, structural engineering and fire safety. The international CRRB conference further broadens the opportunities to compare approaches to building rehabilitation and to establish cooperation with colleagues from abroad.

I consider the integration of high-quality diagnostics with the design of rehabilitation measures and the subsequent verification of their effectiveness to be particularly important. When rehabilitating buildings, we seek solutions that extend their service life, respect the properties of original materials and enable the efficient use of existing structures. It is precisely through open discussion of research findings and practical experience that we can assess the suitability of individual approaches.

At the international level, WTA International continues its work on the preparation and updating of technical guidelines. This year's new publications include Guideline 3-20 on the rehabilitation of historic brick masonry, as well as new documents in Series 11 addressing fire safety in existing and historic buildings, specifically special structures and the classification of existing building elements. Draft guidelines addressing rendering systems for building rehabilitation, mould growth on timber, radon in existing buildings, and the investigation and assessment of masonry properties have also been made available for expert review. These documents provide our professional community with an opportunity to contribute Czech experience to the international discussion.

Supporting the next generation of experts remains an important part of WTA's activities. In addition to the Czech competition for the best Master's and doctoral theses, young professionals also have an opportunity to gain international recognition through the WTA Young Professionals Award. In 2026, the award was presented for the first time in the Practical category, which I particularly welcome as recognition of high-quality practical work. Applications for the 2027 edition may be submitted until 30 November 2026.

I would also like to invite you to the special WTA-Tage 2027 event, „50 Years of WTA", which will take place on 18–20 March 2027 in Munich. WTA is celebrating the fiftieth anniversary of its foundation in 1976, with the anniversary celebrations culminating in this special March event. The ceremonial celebration is scheduled for 18 March at Nymphenburg Palace. The programme will also include the WTA International General Assembly, a technical colloquium and a final technical excursion. I hope that we will be represented there by a strong Czech delegation and that we will have the opportunity to celebrate together the importance of international cooperation in building rehabilitation and heritage conservation.

In conclusion, I would like to thank all WTA CZ members, authors, organisers and partners for their work and continued support. I wish you inspiring conference sessions, fruitful discussions and pleasant personal encounters here in Brno. I look forward to our continued cooperation..

Prof. Ing. Rostislav Drochytka, CSc., MBA, dr. h. c.
Chairman of WTA CZ

WTA V ČESKÉ REPUBLICE

Činnost je obdobná jako ve WTA International, pokrývá 10 pracovních skupin a v roce 2026 **Rada WTA CZ** pracuje ve složení:

Předseda:
prof. Ing. Rostislav Drochytka, CSc., MBA, dr. h. c., VUT v Brně, Fakulta stavební, Veveří 95, 602 00 Brno
tel.: 541 147 500, 608 503 938, e-mail: rostislav.drochytka@vut.cz

Místopředseda spolku, pověřený radou spolku:
doc. Ing. Pavel Reiterman, Ph.D., Experimentální centrum FSv ČVUT, Thákurova 7, 166 29 Praha 6
tel.: 224354 376, e-mail: pavel.reiterman@fsv.cvut.cz

Dozorčí rada:
doc. Ing. Eva Burgetová, CSc. – předseda dozorčí rady, ČVUT Praha, FSv, Thákurova 7, 166 29 Praha 6, tel. 224 354 681
Ing. Jindřich Melichar, Ph.D., VUT v Brně, Fakulta stavební, Veveří 95, 602 00 Brno, tel. 541 147 463
doc. Ing. Karel Šuhajda, Ph.D., VUT v Brně, Fakulta stavební, Veveří 95, 602 00 Brno, tel. 541 147 463

Členové:
Ing. Petr Čeliš, Realsan Group s.r.o., Mrštíkova 399/2a, Liberec III – Jeřáb, PSČ 460047, tel.: 485 246 501-3
doc. Ing. Vít Černý, Ph.D., VUT v Brně, Fakulta stavební, Veveří 95, 602 00 Brno, tel. 541 147 463
Ing. Pavel Dohnálek, Ph.D., Betosan, s.r.o., Na dolinách 28, 147 00 Praha 4, tel.: 602 149 443
Ing. arch. Karel Doubner, Chodská 17, 120 00 Praha 2, tel.: 603 433 611
Ing. Aleš Jakubík, Ph.D., Redrock Construction s. r. o., Karolinská 654/2, Praha 8 - Karlín, CZ-18600, tel.: 283 893 533
prof. Ing. Jiří Kolísko, Ph.D., ČVUT Praha, Kloknerův ústav, Šolínova 7, 166 08 Praha 6, tel.: 224 353 537
prof. Ing. Miloslav Novotný, CSc., VUT v Brně, Fakulta stavební, Veveří 95, 602 00 Brno, tel.: 541 147 409
Ing. Tomáš Plicka, MC-Bauchemie s.r.o., Skandinávská 990, 267 53 Žebrák, tel.: 311 545 155
Ing. Pavel Šťastný, CSc., Remmers s.r.o., Technická 2247, 251 01 Říčany u Prahy, tel.: 323 604 877

Dalšími členy Rady WTA CZ jsou níže uvedení vedoucí odborných pracovních skupin (OPS)

Odborné pracovní skupiny

Pracovní skupina	Odborné zaměření	Vedoucí referátu	Pracoviště	Telefon / e-mail
Pracovní skupina 1	Sanace a ochrana dřeva	doc. Ing. Jan Vaněrek, Ph.D.	VUT v Brně, fakulta stavební Veveří 95, 602 00 Brno	605 449 831 jan.vanerek@vut.cz
Pracovní skupina 2	Povrchové úpravy	Ing. Radka Navrátilová, Ph.D.	Kloknerův ústav ČVUT v Praze Šolínova 7, 166 08 Praha 6	777 683 727 radka.navratilova@cvut.cz
Pracovní skupina 3	Přírodní a umělý kámen	RNDr. Kateřina Krutilová, Ph.D.	Zkušebna kamene a kameniva Husova 675, 508 01 Hořice	604 747 968 ao@zkk.cz
Pracovní skupina 4	Sanace a ochrana zdiva	Ing. Jaroslav Pánik	Sanace a vysoušení staveb s.r.o. Otická 32, 746 01 Opava	603 158 612 info@sanace-staveb.cz
Pracovní skupina 5	Sanace a ochrana betonu	doc. Ing. Pavel Reiterman, Ph.D.	Experimentální centrum FS ČVUT Thákurova 7, 166 29 Praha 6	224 354 376 pavel.reiterman@fsv.cvut.cz
Pracovní skupina 6	Fyzikálně-chemické zásady	doc. Ing. Jiří Bydžovský, CSc.	VUT v Brně, fakulta stavební Veveří 95, 602 00 Brno	603 416 247 jiri.bydzovsky@vut.cz
Pracovní skupina 7	Analýza únosnosti staveb	doc. Ing. Petr Fajman, CSc.	ČVUT v Praze, fakulta stavební Thákurova 7, 166 29 Praha 6	224 354 477 fajman@fsv.cvut.cz
Pracovní skupina 8	Hrázděné a roubené stavby	Ing. Pavel Šťastný, CSc.	Remmers CZ s.r.o. Technická 22247, 251 01 Říčany	323 604 877 pavel.stastny@remmers.com
Pracovní skupina 9	Požární ochrana	Ing. Petr Beneš, CSc.	VUT v Brně, fakulta stavební Veveří 95, 602 00 Brno	541 147 405 petr.benes@vut.cz
Pracovní skupina 10	Ocel a sklo	prof. Ing. Martina Eliášová, CSc.	ČVUT v Praze, fakulta stavební Thákurova 7, 160 00 Praha	224 354 921 eliasova@fsv.cvut.cz

Sekretariát společnosti:
Ing. Helena Šubrtová, Novotného lávka 5, 116 68 Praha 1, tel.: 221 082 397, e-mail: wta@wta.cz

HOLLOWED HERITAGE – DETERIORATION OF DOBŘÍŠ HISTORIC STONE BRIDGE AFTER INCOMPATIBLE REPAIR

OHROŽENÉ HISTORICKÉ DĚDICTVÍ – DEGRADACE HISTORICKÉHO KAMENNÉHO MOSTU V DOBŘÍŠI V DŮSLEDKU POUŽITÍ NEVHODNÝCH OPRAVNÝCH MATERIÁLŮ

*BAUEROVÁ Pavla[1, a *], FRANKEOVÁ Dita[1], NÁHUNKOVÁ Pavla[1] and SLÍŽKOVÁ Zuzana*

Abstract
The study examines the historic stone bridge in Dobříš, Central Bohemia, built in 1830 and recently declared a cultural monument. During planned repairs, the internal masonry was found to be so degraded that it required almost complete replacement. Characterization of the original granite bedding mortar by thermal analysis, light microscopy and SEM revealed a low lime content, under-fired lime grains, unsorted river sand and iron-rich slag probably originating from local hammer mills. Although this weak mortar functioned for nearly two centuries, a 1960s shotcreate repair sealed the structure, disrupted moisture transport and promoted water accumulation, leading to severe deterioration.

Abstrakt
Studie se zabývá historickým kamenným mostem v Dobříši ve středních Čechách, který byl postaven v roce 1830 a nedávno prohlášen za kulturní památku. Při plánované opravě bylo zjištěno, že vnitřní zdivo mostu je natolik degradované, že vyžaduje téměř úplnou výměnu. Charakterizace původní granitové zdicí malty pomocí termické analýzy, světelné mikroskopie a rastrovací elektronové mikroskopie (SEM) odhalila nízký obsah vápna, nedopálená vápenná zrna, netříděný říční písek a strusku s vysokým obsahem železa, která pravděpodobně pochází z místních hamrů. Přestože tato málo kvalitní malta plnila svou funkci téměř dvě století, oprava provedená v 60. letech 20. století pomocí stříkaného betonu (torkretu) konstrukci uzavřela, narušila transport vlhkosti a podpořila hromadění vody, což vedlo k výrazné degradaci konstrukce.

Key words: *bridge; deterioration; mortar; microscopy.*

1. INTRODUCTION

The historic stone bridge over the Pilský Stream in Dobříš, dating from the 1830s, represents a significant masonry structure whose preservation has recently become the subject of conservation and material research (Fig. 1). Originally threatened with demolition due to its emergency condition, the bridge was instead listed as a cultural monument [1]. During the subsequent repair works, however, the internal structure was found to be severely degraded, requiring almost complete dismantling and replacement of the core, while the original stone material was reused as the external facing.

In the reconstruction of historic bridges, practice often prioritizes the functional performance of repaired masonry over its historical value. At the same time, the design of newly applied bedding and pointing mortars is usually based on a general notion of historic mortars and on assumptions about their replacement with contemporary compatible materials, typically hydraulic lime modified with white Portland cement, rather than on a detailed material characterization of the specific structure.

However, through the hollowing-out of the bridge – removing its original internal fabric and replacing it with a functional reinforced-concrete core – the structure loses a substantial part of its historical memory, including information on the material and technological aspects of the original construction. A detailed material survey based on microscopic methods can preserve at least part of this memory. It should therefore form an integral part of the planning of conservation interventions, particularly for bridges listed as cultural monuments.

This study presents the material characterization of three mortar samples taken from different parts of the bridge: two bedding and one pointing mortar. The aim was to determine the composition and technological characteristics of the original mortars and thus contribute to the systematic documentation and mapping of materials used in 19th and 20th century masonry bridges.

2. MATERIALS AND METHODS

Three mortar samples from different parts of the bridge were analyzed. The samples were designated as follows:

- KMD-1 – masonry mortar from the interior of the bridge
- KMD-3 – masonry mortar
- KMD-5 – pointing mortar



Fig. 1. *Stone bridge in Dobříš: (a) view of the dismantled bridge from the southwest; (b) remnant of the masonry arch; (c) detail of the bedding mortar in the bridge arch; (d) view of the dismantled bridge from the northeast; (e) overall view of the reconstructed bridge from the northwest; (f) detail of the outer masonry built from the original stones and repointed with new mortar.*

The mortar samples were examined using optical microscopy, scanning electron microscopy with energy-dispersive spectroscopy (SEM-EDS), cathodoluminescence (CL), and thermogravimetric analysis (TGA). Polished sections embedded in epoxy resin were observed in reflected light using an Olympus BX53M microscope and, after carbon coating, analyzed with a Tescan MIRA II LMU scanning electron microscope equipped with a Bruker EDS detector at an accelerating voltage of 15 kV and a working distance of 15 mm.

Cathodoluminescence observations were performed under cold-cathode excitation using an Olympus BX53M polarizing light microscope fitted with an Olympus DP74 digital camera and a CITL Mk 5-2 cold-cathode system. The method was used to distinguish carbonate particles representing residues from lime production (so called "lime lumps") from limestone added as aggregate.

The binder's chemical and phase composition was further assessed by TGA using a TA Instruments SDT 650 over a temperature range of 25–1,000 °C in a nitrogen atmosphere at a heating rate of 20 °C/min. For thermal analysis, the mortar was gently crushed, sieved through a 0.063 mm mesh, and the resulting fine fraction was analyzed.

3. RESULTS

3.1. Microscopy

Based on the microscopic examination, the studied mortars are very similar in both microstructure and chemical composition (Tab. 1) and can therefore be considered the same material. In all samples, natural sand was used as aggregate, consisting of rounded quartz grains and rock fragments containing feldspars and other silicate minerals. In addition to sand, the mortars contain substantial amounts of apparently heat affected limestone fragments and metallurgical slag particles, frequently exceeding 5 mm in size (Fig. 2).

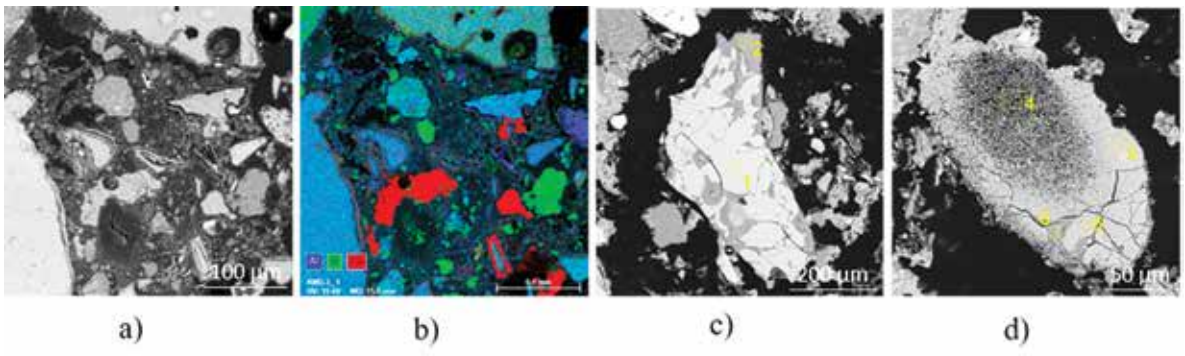


Fig. 2. *Scanning electron micrographs showing typical microstructure od mortars with slag grains and lime lumps – (a) KMD-3 sample in BSE regime and (b) EDS elemental map showing the distribution of Ca (red), Si (green) and Al (blue); (c, d) KMD-5 sample – details of limestone fragments (lumps). The areas from which EDS spectra 1–6 were acquired are outlined in yellow (see Tab. 1).*

Tab. 1. *Average chemical compositions of the binders and slag particles in mortars KMD-1 and KMD-3 (based on at least four measurements), and the chemical composition of technological particles in sample KMD-5.*

Spectrum	CaO	SiO_2	Al_2O_3	MgO	Na_2O	K_2O	SO_3	Cl	P_2O_5	FeO	TiO_2	MnO
KMD-1_ binder_ average	19.8	53.8	15.0	1.1	1.5	1.3	2.4	0.9	0.7	3.7	-	1.4
KMD-3 binder_ average	14.8	56.0	16.7	1.0	1.7	1.5	2.9	3.0	-	3.0	-	1.3
KMD-1 slag_average	8.2	51.9	26.4	0.6	0.2	5.4	-	-	-	5.2	1.3	2.4
KMD-3 slag_average	13.8	52.2	20.0	1.7	0.6	3.0	1.0	0.6	-	6.5	1.6	0.7
KMD-5_ 6_lump	-	100.0	-	-	-	-	-	-	-	-	-	-
KMD-5_ 5_lump	97.9	1.1	0.5	0.5	-	-	-	-	-	-	-	-
KMD-5_ 4_lump	94.7	3.1	1.2	1.1	-	-	-	-	-	-	-	-
KMD-5_ 3_lump	99.2	0.8	-	-	-	-	-	-	-	-	-	-
KMD-5_2_lump	-	100.0	-	-	-	-	-	-	-	-	-	-
KMD-5_ 1_lump	5.5	52.2	25.4	1.0	-	5.3	-	-	-	9.6	1.0	-

3.2 Cathodoluminescence

Although the limestone fragments showed signs of thermal alteration under the electron microscope, cathodoluminescence provided conclusive evidence that they were overburnt technological particles associated with the relatively poor-quality firing of the lime used, rather than aggregate particles. Fig. 2 displays the results of cathodoluminescence observations.

Cathodolminescence method makes it possible to distinguish between thermally unaltered limestone material, which exhibits red luminescence, and pyrogenic carbonate particles exposed to high temperatures, which show no luminescence and therefore appear black [2]. Since the limestone particles in the mortars studied exhibited no luminescence, i.e. they did not emit red light (Fig. 3), they must represent binder-related fragments of the original limestone that had undergone thermal treatment.

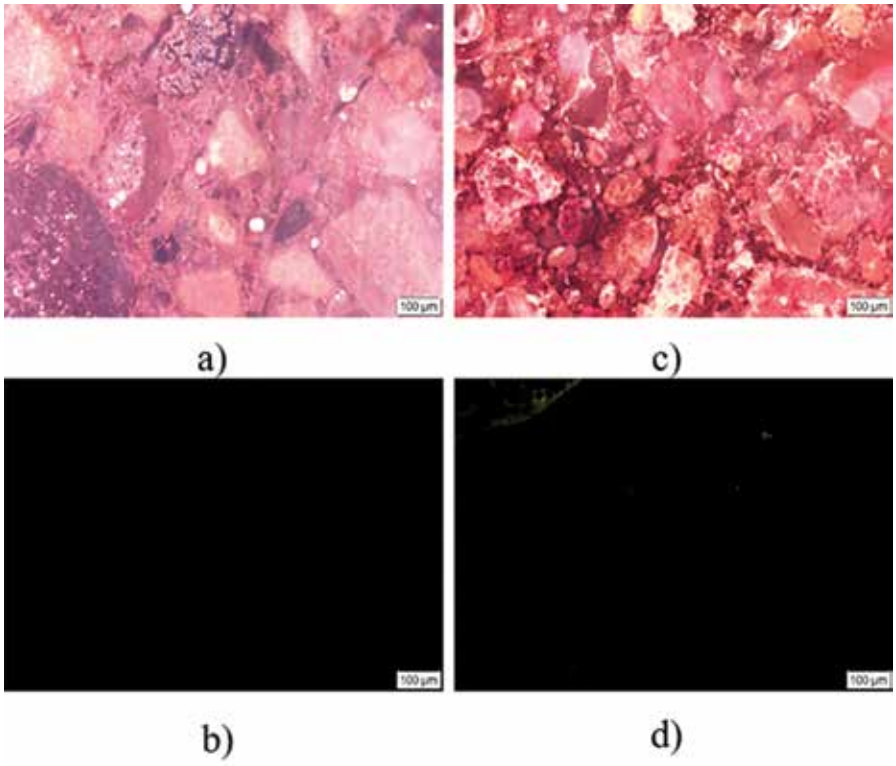


***Fig. 3**. Light microscope (up) and cathodoluminescence (bottom) images of the mortars – KMD-1 (a,b); KMD-5 (c,b).*

3.3. Thermal analysis

The principal process occurring during the heating of all three samples was the decomposition of calcium carbonate, with a maximum between 700 and 800 °C (Fig. 4). The amount of carbon dioxide released during decomposition corresponded to a calcium carbonate content of 21.8–50.9 wt.% in the binder fraction (Tab. 2). Mortars KMD-1 and KMD-5 contained approximately twice as much calcium carbonate as mortar KMD-3, which was sampled from the interior of the pier. By contrast, KMD-3 exhibited a higher weight loss in the temperature range of 50–600 °C, associated with the release of chemically bound water, most likely from hydraulic phases or clay minerals.

***Tab. 2.** Weight loss and $CaCO_3$ content assed by thermal analysis.*

sample	weight loss (%)			$CaCO_3$ content (% hm.)
	50-200°C	200-600°C	600-950°C	
KMD 1	2,17	4,36	19,2	43,6
KMD 3	5,01	5,15	9,61	21,8
KMD 5	1,18	4,37	22,4	50,9

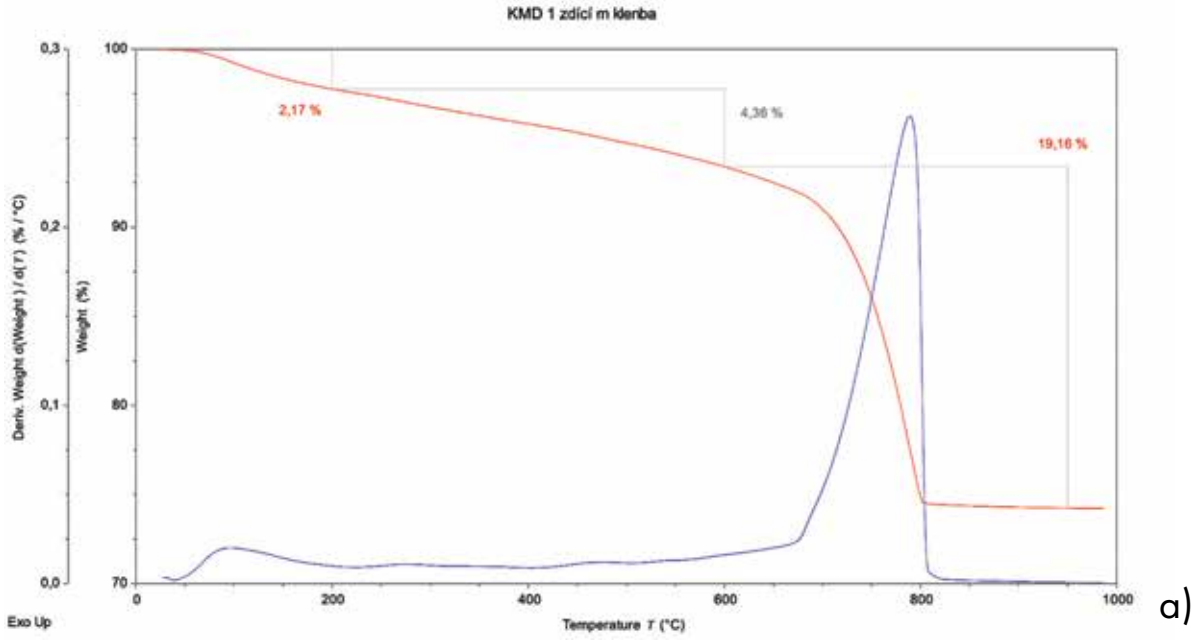
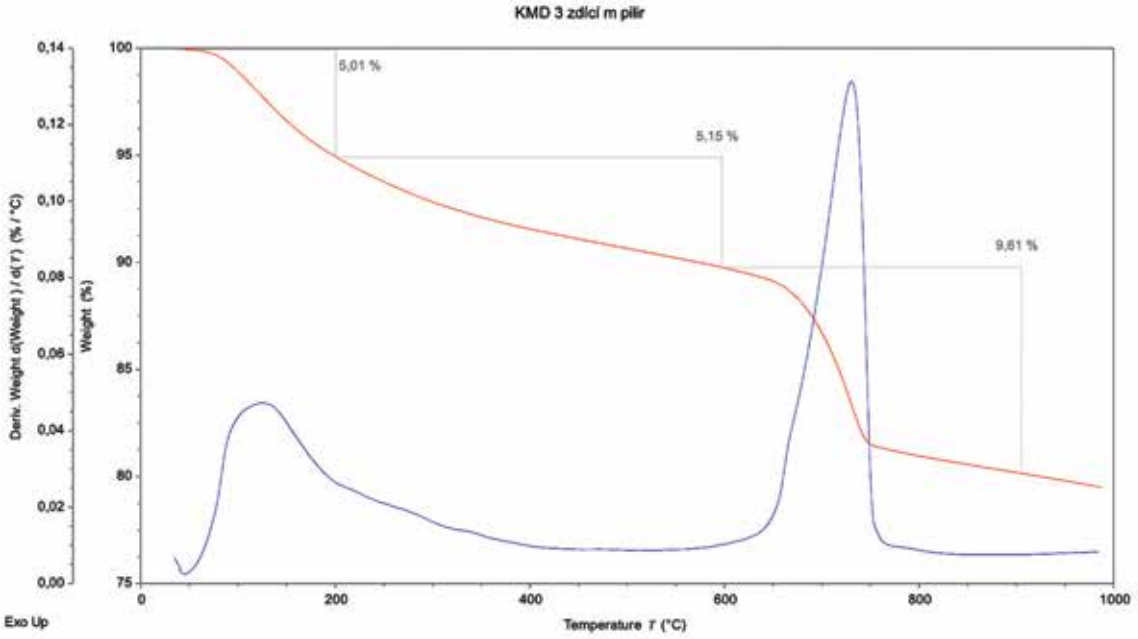
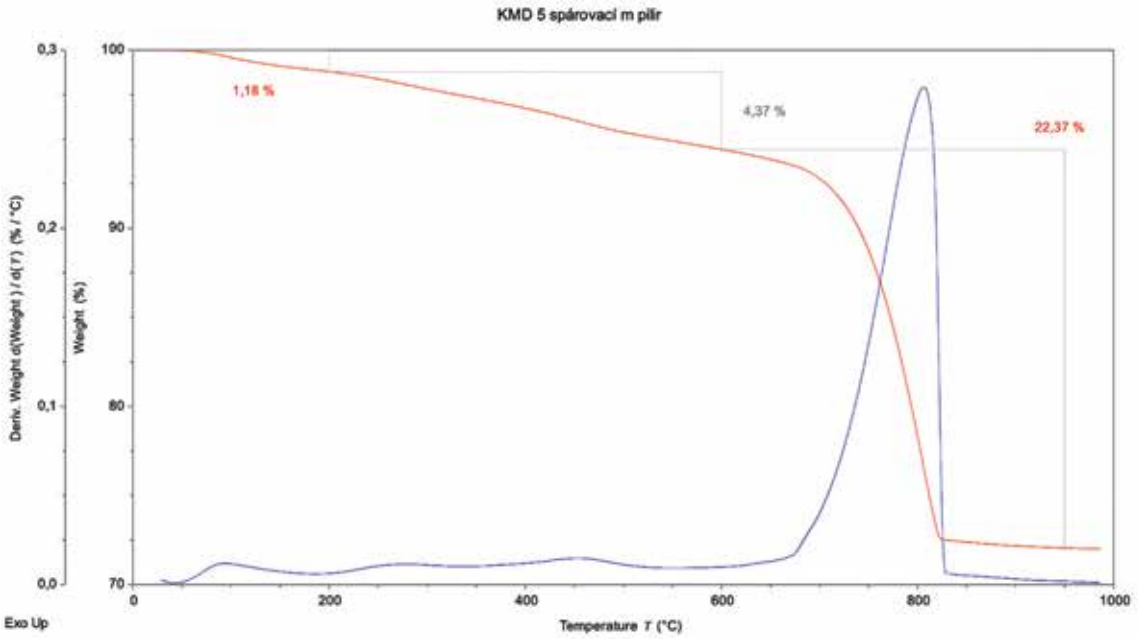


***Fig. 4.** Thermogravimetric curves of the mortars – (a) KMD-1, (b) – KMD-3, (c) KMD-5.*



b)



c)

4. DISCUSSION

As seen from the results, mortars studied exhibit very similar characteristics and were produced using the same raw materials. Their binder is hydraulic but contains no relics of clinker minerals. All samples include numerous binder-related particles (lime lumps), which are characteristic of the original raw material from which the binder (i. e. hydraulic lime) was produced (Fig. 2c,d). Their high abundance indicates poorely controlled firing conditions, particularly insufficient and uneven temperature distribution within the kiln, resulting in lower-quality lime. Most of these particles consist of thermally fractured fragments of the original raw material, identified as siliceous limestone. However, SiO_2 is not homogeneously distributed within the rock but occurs in clearly defined domains. A similar feature is observed in several Paleozoic chert-bearing limestone lithotypes from the Barrandian area [3], the nearest potential source of raw material for lime production. Their unambiguous identification in the studied mortars would, however, require further analytical investigation.

Metallurgical slag is also present in the mortars in substantial quantities. It remains uncertain whether the slag was added merely as a locally available recycled aggregate which, owing to its pozzolanic properties, inadvertently imparted hydraulic characteristics to the mortar, and/or whether it was used deliberately to improve the mechanical, particularly strength-related, properties of the material. Iron ore from the Brdy region had already been processed in the Stará Huť area since the 18th century [4], making slag a readily available local material. In a moist environment, the slag reacts with the carbonate binder of the mortar to form hydraulic products, particularly C–S–H gels, which increase mortar strength [5]. Experiments involving the addition of slag to mortars had been carried out in Europe as early as

the seventeenth century [6]. Nevertheless, we consider it more likely that the slag was primarily used as a readily and economically available aggregate. Even so, by incorporating slag into the mortar, the local masons were somewhat ahead of their time, as blast-furnace slag cement did not begin to be manufactured industrially in the Czech lands until 1890 [7].

The proportion of the lime component, expressed as $CaCO_3$, in the binder is relatively low, at approximately 50 wt.%. However, the exact original composition cannot be determined due to the advanced degradation of the binder. Prolonged exposure to water probably resulted in the leaching of calcium ions into solution and their subsequent removal, which is reflected in the analytical results by the reduced CaO, or $CaCO_3$, content.

Despite inappropriate reconstruction interventions carried out in the past, the bridge remained in service until 2020. The decisive factor in its deterioration was the layer of shotcrete applied in the 1960s. By sealing the original mortars beneath an impermeable concrete layer, this intervention disrupted the natural circulation and evaporation of water. Moisture consequently accumulated within the bridge structure and contributed to its catastrophic condition, which ultimately necessitated the complete replacement of the internal parts of the bridge.

5. CONCLUSION

The three investigated bedding and pointing mortars were essentially identical in composition and exhibited hydraulic characteristics. They were made of hydraulic lime, sand and local metallurgical slag. Numerous thermally altered particles originating from the raw material used for lime production were identified. The severe, visually apparent deterioration of the mortars was markedly accelerated by the application of dense shotcrete in the 1960s, which restricted natural water circulation and evaporation and promoted moisture accumulation within the bridge structure.

The results demonstrate that the original mortars were not merely functional components of the masonry, but valuable historical materials preserving evidence of local raw materials, lime-burning technology, metallurgical activity, construction practice, and the subsequent transformation of the structure over time. Once the interior of a bridge is hollowed out and discarded, this material record is irreversibly lost. A detailed material investigation should therefore never be omitted and must be undertaken before any intervention involving the removal of the original masonry fabric. Wherever technically feasible, conservation strategies should seek to preserve the historic internal structure and avoid its wholesale replacement with a new reinforced-concrete core. Less invasive approaches, respecting both the functional requirements of the bridge and the material authenticity of its historic fabric, should be preferred.

Even where the preservation of the original core is demonstrably no longer possible, its systematic documentation and material characterization must precede its removal, allowing at least part of the information embodied in the structure to be retained. In this sense, microscopic and physicochemical analysis does more than characterize a mortar: it preserves fragments of the bridge's historical memory before the material in which that memory is written disappears.

6. REFERENCES

[1] Most přes Pilský potok. Památkový katalog. NPÚ. Available online: https://pamatkovykatalog.cz/most-pres-pilsky-potok-22275144 (accessed 20-07-2026).

[2] Ricci, G.; Secco, M.; Addis, A. et al. Integrated multi-analytical screening approach for reliable radiocarbon dating of ancient mortars. Sci Rep 12, 2022, 3339. https://doi.org/10.1038/s41598-022-07406-x

[3] Kozlovcev, P. Vliv mineralogického složení suroviny na vznik fází při výpalu hydraulického vápna a přírodního cementu. (Influence of the mineralogical composition of raw material on phases formed during. the burning of hydraulic lime and natural cement) Dissertation thesis. Faculty of Science, Charles University, Prague, 2018.

[4] Litochleb, J., Černý; P.; Sejkora, J.; Šreinová, B.; Korba, M. Ložiska a výskyty nerostných surovin na území brdských Hřebenů a v jejich okolí (střední Čechy). Bull. mineral.-petrolog. Odd. Nár. Muz. 20, 2012, 2, 129-176

[5] Moranville-Regourd M.; Kamali-Bernard, S. Cements made from blast furnace slag. In Lea´s chemistry of cement and concrete, 5th ed; Hewlett, P. C.; Liska, M., Eds.; Elsevier: Oxford, UK; pp. 469-507.

[6] G. Lindqvist, J.E..; Balksten, K.; Fredrich, B. Blast furnace slag in historic mortars of Bergslagen, Sweden. In: J.I. Álvarez, J.M. Fernández, Í. Navarro, A. Durán, R. Sirera (Eds.), Proceedings of the 5th Historic Mortars Conference, RILEM Publications S.A.R.L., Paris, 2019, pp. 585–595.

[7] Láník, J. Velký příběh. 120 let Královdvorské cementárny 1889-2009, 1st ed., Českomoravský cement, a.s., Prague, 2009.

Authors:

Mgr. Pavla Bauerová, Ph.D. – Department of Materials Research, Institute of Theoretical and Applied Mechanics, CAS, v.v.i., Prosecká 76, 190 00 Praha 9, Czech Republic

Mgr. Dita Frankeová, Ph.D. – Department of Materials Research, Institute of Theoretical and Applied Mechanics, CAS, v.v.i., Prosecká 76, 190 00 Praha 9, Czech Republic

Ing. et Bc. Pavla Náhunková – Department of Materials Research, Institute of Theoretical and Applied Mechanics, CAS, v.v.i., Prosecká 76, 190 00 Praha 9, Czech Republic

doc. Ing. Zuzana Slížková, Ph.D. – Department of Materials Research, Institute of Theoretical and Applied Mechanics, CAS, v.v.i., Prosecká 76, 190 00 Praha 9, Czech Republic

ACKNOWLEDGEMENTS

The research was carried out with the support of the Czech Ministry of Culture as a contribution to project NAKI III DH23P03OVV024. Authors higly appreciate the help of Dr. Petr Kozlovcev with the cathodoluminescence measurements. The text was refined by Chat GPT.

FINITE ELEMENT ASSESSMENT OF A COMPOSITE ROOF WATERPROOFING SYSTEM UNDER COMBINED ENVIRONMENTAL LOADING

POSOUZENÍ KOMPOZITNÍHO STŘEŠNÍHO HYDROIZOLAČNÍHO SYSTÉMU METODOU KONEČNÝCH PRVKŮ PŘI KOMBINOVANÉM PŮSOBENÍ VLIVŮ PROSTŘEDÍ

*Narges Azadvar[1] *, William Jack Finley[2], Maurizio Guadagnini[1,3] and Iman Hajirasouliha[1]*

[1] School of Mechanical, Aerospace and Civil Engineering, Faculty of Engineering, The University of Sheffield, Sheffield, UK

[2] Roberts Group Company, Flint, Wales, UK

[3] Department of Architecture, Construction Engineering and the Built Environment, Politecnico di Milano – polimi, Milan, Italy

Abstract:

This paper presents a finite element investigation of a multi-layer liquid-applied waterproofing system for flat-roof applications under service, ultimate, extreme wind and deformation demands. Eight numerical models were developed in ABAQUS in two phases. The first phase considered a full-scale generic timber-framed masonry building with a plywood roof deck, selected as a conservative structural configuration because of its relatively high flexibility. The models incorporated experimentally derived properties for the waterproofing layers and were subjected to combinations of dead, live, snow, wind and thermal actions. The maximum in-plane strains were compared with the adopted strain-at-break values to quantify safety margins. For full composite action, factors of safety against fracture ranged from 14 to 27; when the critical waterproofing layer was assessed independently, values remained between 10 and 18. The second phase examined a detailed parapet configuration under pressure and suction and assessed deformation compatibility against seismic drift limits. Suction governed the parapet response, but fracture initiation occurred only at loads substantially above the design demand. The results indicate that, for the configurations studied, failure is more likely to be governed by excessive deformation of the supporting structure than by fracture of the waterproofing system.

Abstrakt

Tento článek představuje analýzu vícevrstvého hydroizolačního systému aplikovaného v kapalné formě pro použití na plochých střechách, provedenou metodou konečných prvků. Posuzovány byly požadavky vyplývající z běžného provozu, mezního stavu únosnosti, extrémního zatížení větrem a deformací. V programu ABAQUS bylo ve dvou etapách vytvořeno osm numerických modelů. První etapa zahrnovala model budovy s dřevěným nosným rámem a zděnými stěnami v reálném měřítku, se střešním základem z překližky. Tato konstrukční varianta byla zvolena jako konzervativní řešení vzhledem ke své relativně vysoké poddajnosti. V modelech byly použity vlastnosti jednotlivých hydroizolačních vrstev stanovené na základě experimentálních měření. Konstrukce byla zatížena kombinacemi stálého, užitného, sněhového, větrného a teplotního zatížení. Maximální poměrná přetvoření v rovině vrstev byla porovnána s uvažovanými hodnotami přetvoření při přetržení, aby bylo možné stanovit bezpečnostní rezervy. Při předpokladu plného spolupůsobení jednotlivých vrstev se součinitel bezpečnosti proti porušení tahem pohyboval v rozmezí 14 až 27. Při samostatném posouzení kritické hydroizolační vrstvy zůstaly tyto hodnoty v rozmezí 10 až 18. Druhá etapa se zaměřila na podrobný model konstrukčního řešení atiky, který byl posuzován při působení tlaku a sání větru. Současně byla hodnocena kompatibilita deformací s mezními hodnotami seizmického posunu. Rozhodujícím zatížením pro odezvu atiky bylo sání větru, avšak k iniciaci porušení došlo až při zatíženích výrazně převyšujících návrhové hodnoty. Výsledky ukazují, že u zkoumaných konstrukčních řešení je pravděpodobnější příčinou poruchy nadměrná deformace nosné konstrukce než přetržení samotného hydroizolačního systému.

Keywords: *Composite waterproofing system; Finite element analysis; Roof structures; wind loading; seismic drift; Eurocode-based loading.*

1. INTRODUCTION

Liquid-applied waterproofing systems are a critical component of the building envelope, particularly in flat and low-slope roofs where snow, temperature variations, wind actions and structural movements can influence long-term performance. Unlike prefabricated sheet membranes, liquid-applied systems are applied in situ to form a continuous waterproofing membrane, offering advantages in terms of continuity, adaptability to complex geometries and deformation capacity. However, their performance depends not only on the mechanical properties of the membrane itself, but also on the ability of the complete waterproofing system to accommodate deformation of the supporting structure without premature cracking or fracture.

Previous studies have shown that the mechanical response of waterproofing systems is strongly influenced by material composition, reinforcement and substrate deformation. Feiteira et al. [1] investigated reinforced and unreinforced liquid-applied roof waterproofing systems and demonstrated the importance of reinforcement and material type on mechanical performance. Other studies on flexible waterproofing membranes have shown that strain localisation, crack-bridging behaviour and deformation capacity can be significantly affected by substrate cracking, temperature and loading conditions [2–4]. Numerical modelling has also been successfully applied to roofing systems. Baskaran et al. [5] used three-dimensional finite element (FE) modelling to investigate roof membrane deformation under wind uplift, while Darwish and ElGawady [6] demonstrated the capability of FE analysis to reproduce the behaviour of membrane-retrofitted roofing systems subjected to wind loading.

Similar deformation-compatibility issues have been widely investigated in externally applied composite strengthening systems. Experimental and numerical studies of other composite systems have demonstrated the importance of composite interaction, deformation capacity and the response of thin composite layers under combined loading [7–9]. Although strengthening systems and waterproofing membranes have different functions and constituent materials, both require compatibility between a relatively thin composite layer and its supporting substrate. These studies therefore provide a useful basis for assessing reinforced waterproofing systems at the structural scale.

Despite previous research on waterproofing materials and membrane behaviour, comparatively limited information is available on the response of multi-layer reinforced waterproofing systems interacting with complete supporting structures under combined environmental and structural loading. In particular, the relationship between global structural deformation, local detailing and strain demand within the waterproofing layers requires further investigation.

This study therefore investigates the performance of the Roberts Group waterproofing system using finite element modelling. A full-scale timber-framed masonry building with a plywood roof deck is first analysed under combinations of dead, live, snow, wind and thermal actions. A detailed parapet model is then used to investigate local strain concentrations under wind pressure and suction and to assess deformation compatibility under imposed lateral drift. The predicted strain demands are compared with experimentally determined strain-at-break values to evaluate the available safety margins and identify the critical loading conditions and locations.

2. MATERIALS AND METHODS

2.1. Waterproofing system and material properties

The assessed system comprises two waterproofing layers, with a glass-fibre reinforcement embedded within the base coat, together with an optional carrier layer over an 18 mm plywood substrate. The carrier layer is substrate-dependent and was included in the numerical models to represent the selected practical build-up. Experimental stress–strain data supplied by Roberts Group were used to define the mechanical properties of the waterproofing system. Measured strain at break for the full composite system ranged from 3.45% to 4.36%; a conservative value of 3.0% was adopted in the analyses.

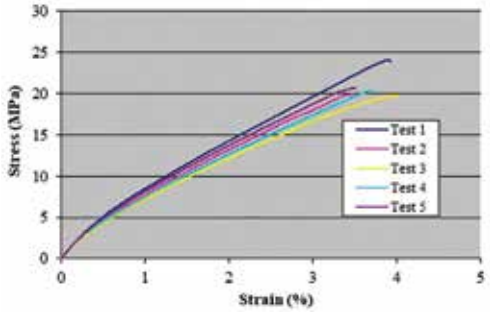


***Figure 1**: System acting as a full composite material: Experimental stress–strain results for Waterproofing with carrier layer*

***Table 1.** Material properties adopted in the finite element models.*

Material		Thickness (mm)	Density (Kg/m^3)	E (GPa)	Poisson's ratio	Thermal expansion coefficient (1/°C)	Elongation to break (%)
Masonry wall		---	2400	25	0.2	5.0×10^{-6}	---
Timber (C24)		---	420	11.2	0.25	3.5×10^{-6}	---
Plywood		18	550	6.1	0.25	4.5×10^{-6}	---
Waterproofing	FW-Water proofing@0.5L/m^2 (Layer 1)	0.5	1250	0.048	0.35	160×10^{-6}	7.0 %
	FW-Water proofing@1.3L/m^2 (Layer 2)	1.5	1350	0.883	0.25	160×10^{-6}	2.0 %
	Elotene DSN carrier (Layer 3)	0.6	1050	0.2	0.4	160×10^{-6}	5.0 %
	Full composite	2.6	1250	0.605	0.35	160×10^{-6}	3.0%

2.2. Full-scale roof model

A full-scale generic roof structure was developed in accordance with the project design assumptions and typical structural dimensions. A timber-framed masonry building with a plywood roof deck was selected because timber framing exhibits larger deformations than comparable reinforced-concrete or steel systems and therefore provides a conservative basis for assessing waterproofing strain demand. Six full-scale FE (Finite Element) models were analysed in Phase 1. The nominal model dimensions were 20.4 m × 25.4 m × 4.1 m, with approximately 217,330 elements.

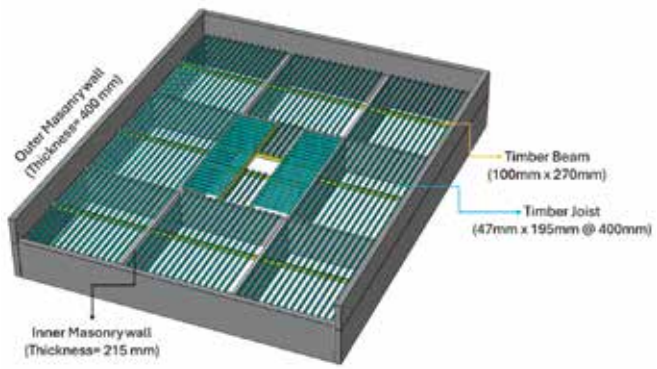


Figure 2: *Full-scale structural system used for the Phase 1 finite element models.*

Masonry walls, timber beams and joists were represented using eight-node reduced-integration solid elements (C3D8R), while the plywood roof deck and waterproofing system were represented using four-node reduced-integration shell elements (S4R). A nominal mesh size of 200 mm was used for the walls, plywood and waterproofing system, with a finer 50 mm mesh for the beams and joists. Mesh sensitivity analyses were undertaken to confirm the reliability of the predicted response. The bases of the masonry walls were fully restrained.

2.3. Loading and assessment procedure

The Phase 1 models were subjected to dead, live, snow, wind and thermal actions based on Eurocode provisions [10–13]. Five Eurocode-based combinations and one client-specified high-wind/high-thermal combination were considered. For each case, the maximum in-plane strain in the waterproofing system was extracted and compared with the relevant strain-at-break value. The factor of safety was defined as the adopted strain at break divided by the maximum predicted strain demand.

Table 2: *Load combinations used in the full-scale analyses.*

Load Combination	Load combinations
1	DL+LL
2	1.35*DL+ 1.50*W+ 0.75*S+ 1.50*LL+0.9*T
3	1.35*DL+ 1.50*S+ 0.9*W+ 1.05*LL+0.9*T
4	1.35*DL+ 1.50*LL+ 0.75*S+0.9*W+0.9*T
5	1.35*DL+ 1.50*T+0.75*S+ 0.9*W+ 1.05*LL
6- Client-Specified	1.5*DL + 1.5*LL + 5.0*W + 0.75*S + 2.0*T

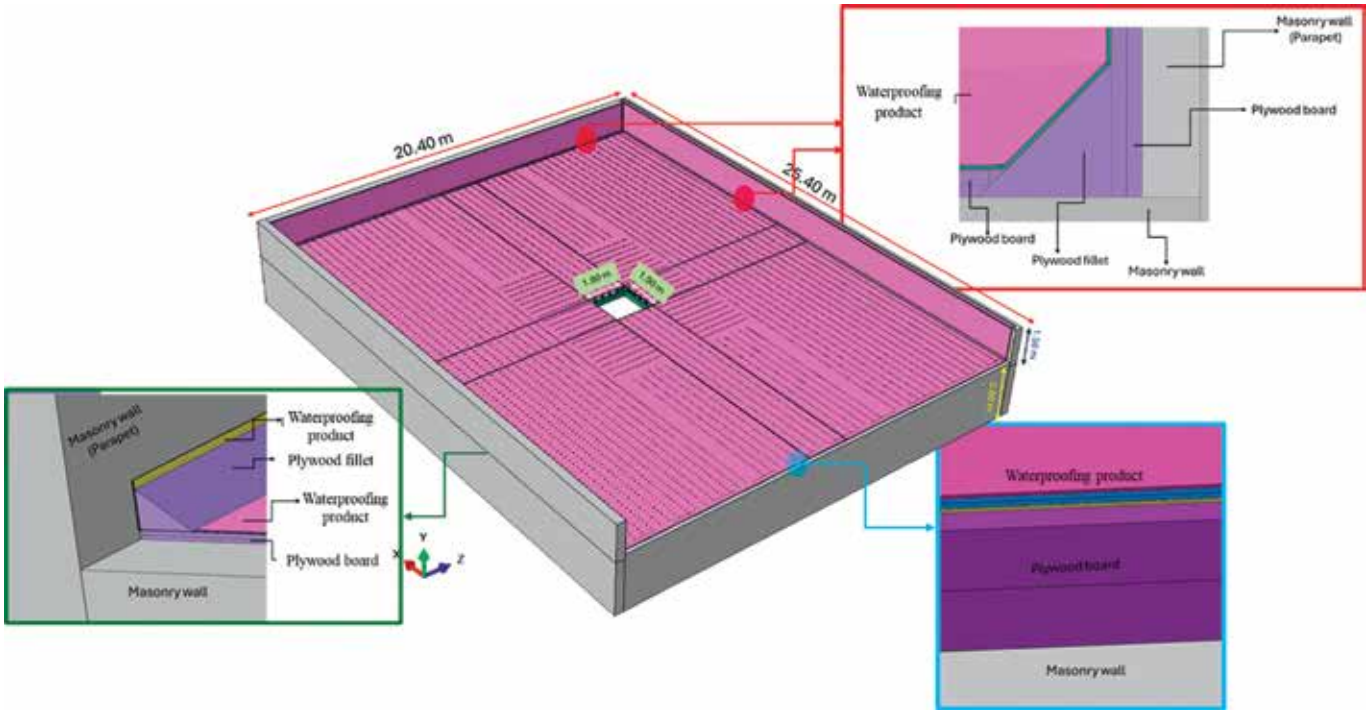


Figure 3: *Representative ABAQUS model showing the roof system and local waterproofing details.*

2.4. Detailed parapet model

Phase 2 focused on a detailed parapet model because Phase 1 identified parapet regions as critical locations for strain concentration. Distributed wind loading was applied to the parapet in both pressure and suction directions using force-controlled analyses. Local strain distributions were evaluated to determine the critical location and the load corresponding to fracture initiation. The same model was also used to investigate deformation compatibility by imposing inward and outward drift and comparing the resulting waterproofing strains with drift limits commonly used for attached non-structural components in Eurocode 8 and ASCE/SEI 7 [14,15].

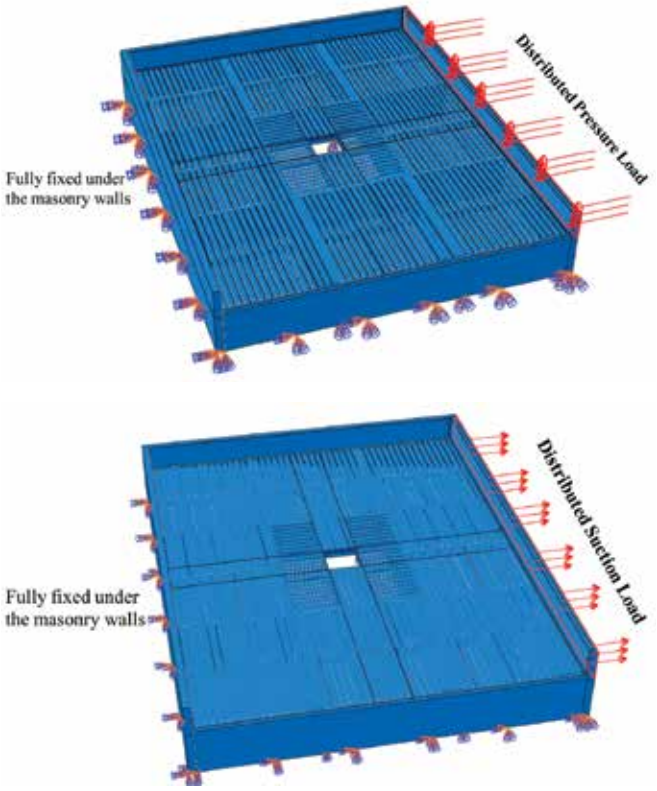
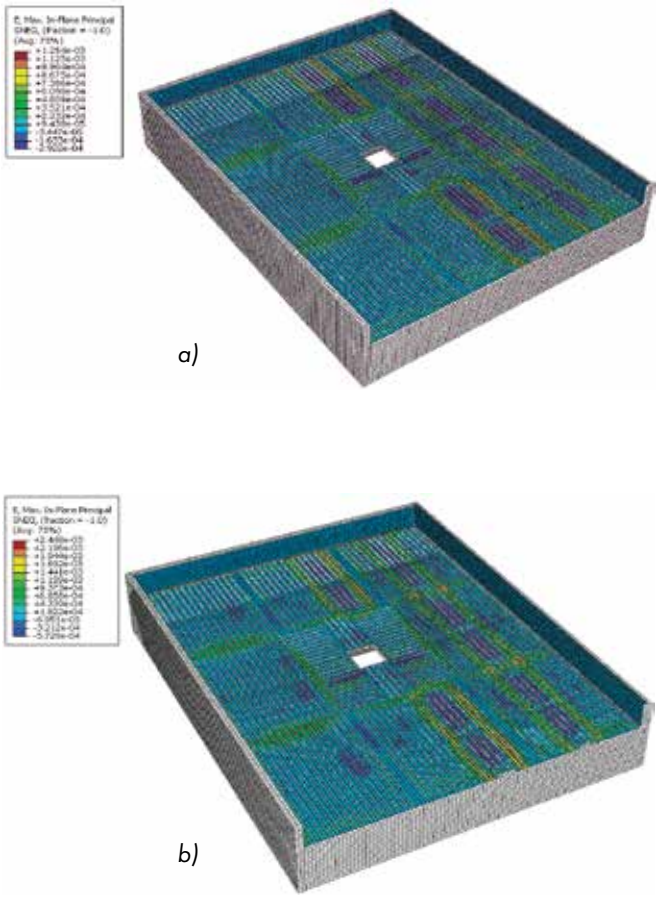


Figure 4: *Detailed parapet model under distributed pressure and suction loading.*

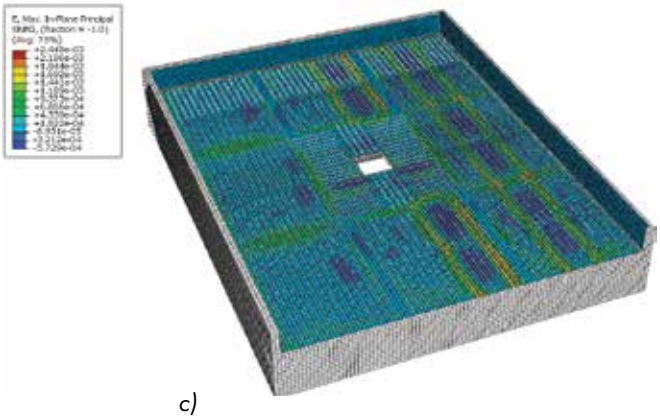
Table 3: *Calculated factors of safety against fracture for Phase 1.*

Load combination	Full composite action	Layer 2
1	27	18
2	15	10
3	15	10
4	15	10
5	18	13
6	14	10



a)

b)

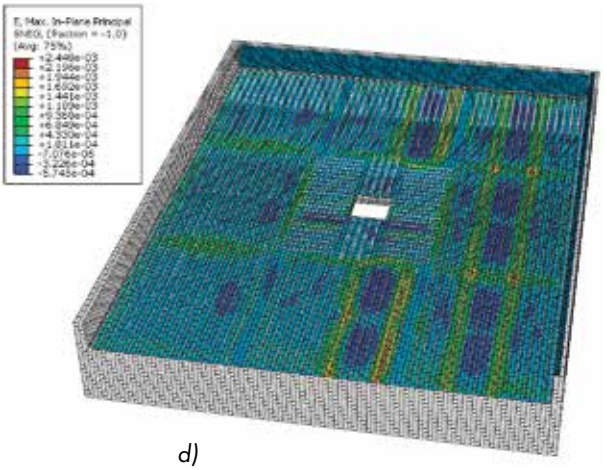


c)

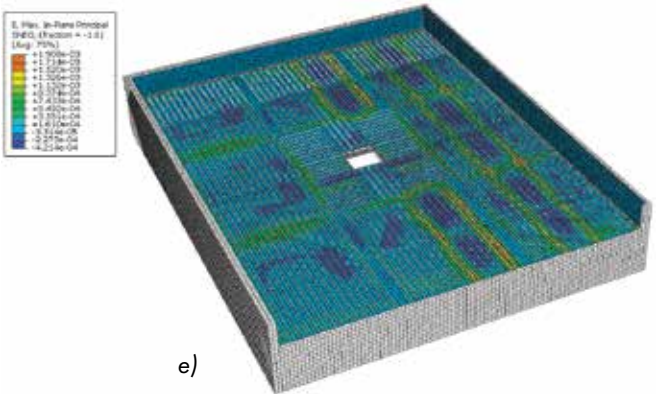
3. RESULTS

3.1. Full-scale roof response

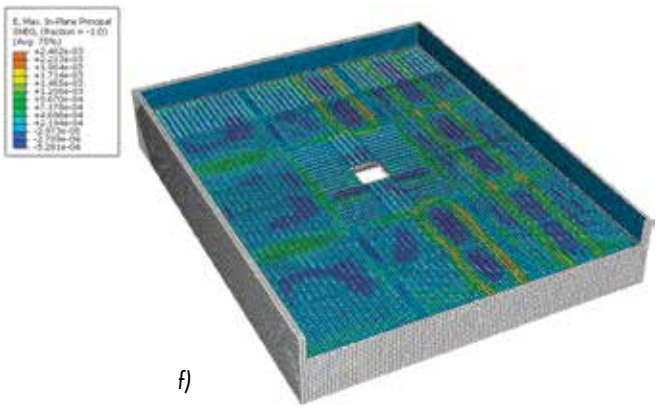
Across all six load combinations, the predicted waterproofing strains remained substantially below the adopted fracture limits. For the full composite system, the calculated factors of safety ranged from 14 to 27. To provide a conservative comparison, Layer 2 was also assessed independently without relying on full composite action; the corresponding factors of safety remained between 10 and 18. The lowest margins occurred for combinations containing the larger wind and thermal contributions, but no fracture was predicted for any of the assessed serviceability or ultimate loading scenarios.



d)



e)



f)

Figure 5: *In-plane strain of models under a) load combination 1, b) load combination 2, c) load combination 3, d) load combination 4, e) load combination 5, and f) load combination 6*

3.2. Parapet response under extreme wind

The detailed analyses showed that the maximum strain and fracture initiation occurred at the fillet corners adjacent to the masonry wall. Fracture initiation was predicted at distributed pressure and suction loads of approximately 253 kN/m² and 41 kN/m², respectively. Suction was therefore the governing direction. Nevertheless, the critical suction load was approximately 58 times the maximum design wind load and 11 times the factored wind load used in the client-specified load combination. These results indicate a substantial reserve against wind-induced fracture when the parapet and supporting structure are properly designed and constructed.

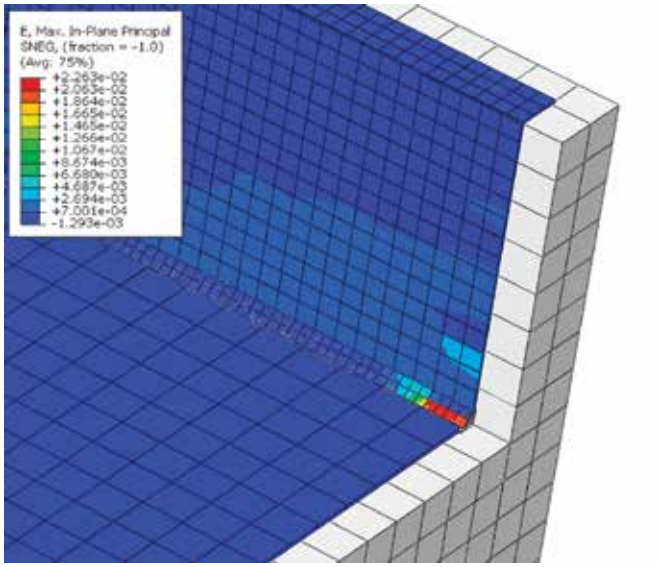


Figure 6: *The result of FE models under distributed suction load*

3.3. Deformation compatibility and seismic drift

In general, allowable drift ratio limits (displacement/height) in seismic regions depend strongly on the type and behaviour of structural and non-structural elements. For buildings with non-structural components attached to the structure, such as parapets, the maximum expected inter-storey drift ratio is typically limited to 0.5% and 1.0% in accordance with Eurocode 8 [14] and ASCE 7 [15], respectively.

For outward deformation, the waterproofing strain demands associated with drift ratios of 0.5% and 1.0% were approximately 0.24% and 0.48%, respectively. For inward deformation, the corresponding demands reduced to approximately 0.04% and 0.08%. Using the conservative 3.0% strain-at-break value for the composite system, the resulting safety factors were greater than 12 relative to the 0.5% Eurocode 8 [14] drift level and greater than 6 relative to the 1.0% ASCE/SEI 7 [15] drift level. The results therefore suggest that the waterproofing system itself is unlikely to constitute the critical vulnerability under the deformation demands considered.

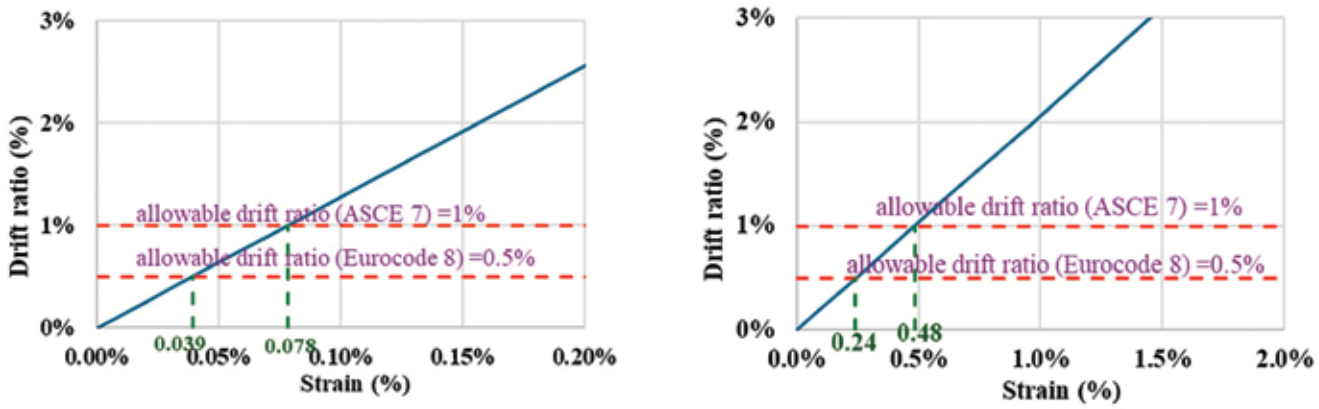


Figure 7: *The allowable drift ratio of FE models under a) inward drift, b) outward drift*

4. DISCUSSION

The analyses consistently show that global roof deformation and local detailing govern the strain demand imposed on the waterproofing system. The use of a timber-framed roof provides a deliberately conservative structural basis because its lower stiffness produces larger substrate deformations than would generally be expected for reinforced-concrete or steel-framed alternatives. Even under this assumption, the calculated safety margins remained high. The comparison between full composite behaviour and the isolated critical layer also demonstrates that the conclusion is not dependent on assuming perfect composite action across the full build-up.

The parapet analyses provide an important local check that is not captured by global roof response alone. Although pronounced strain concentrations developed at the fillet adjacent to the masonry wall, the predicted fracture loads were well above the design-level wind actions. Similarly, the imposed-drift analyses indicate substantial deformation capacity relative to the adopted Eurocode 8 [14] and ASCE/SEI 7 [15] drift limits. Taken together, these findings suggest that, for the configurations considered, excessive deformation or damage of the supporting structure would be expected to precede fracture of the system.

The results should be interpreted within the scope of the numerical assumptions. The models use material properties derived from the available experimental data and idealised representations of interfaces, boundary conditions and construction details. Future work could extend the assessment through dedicated component tests of critical details, explicit modelling of interface debonding and cyclic effects, and validation against full-scale experiments under combined environmental and mechanical loading.

5. CONCLUSION

A numerical assessment of the waterproofing system was undertaken using full-scale roof and detailed parapet FE models. The principal conclusions are:

- The full composite waterproofing system achieved calculated factors of safety against fracture between 14 and 27 under the six assessed load combinations.
- Even when the critical Layer 2 was considered independently, without relying on full composite action, factors of safety remained between 10 and 18.
- The calculated safety factors relative to the adopted Eurocode 8 and ASCE/SEI 7 drift limits were greater than approximately 12 and 6, respectively.
- For the studied configurations, potential system failure is therefore more likely to be associated with excessive deformation or damage of the supporting structural elements than with fracture of the waterproofing layer.

6. REFERENCES

[1] Feiteira, J., Lopes, J. G., & de Brito, J. (2013). Mechanical performance of liquid-applied roof waterproofing systems. Journal of Performance of Constructed Facilities, 27(3), 244–251. https://doi.org/10.1061/(ASCE)CF.1943-5509.0000314.

[2] Waldvogel, M., Zurbriggen, R., Berger, A., & Herwegh, M. (2020). The microstructural evolution of cementitious, flexible waterproofing membranes during deformation with special focus on the role of crazing. Cement and Concrete Composites, 107, 103494. https://doi.org/10.1016/j.cemconcomp.2019.103494.

[3] Waldvogel, M., Zurbriggen, R., Berger, A., & Herwegh, M. (2020). Influences of temperature and opening rate of substrate cracks on the mechanical behaviour, crack-bridging ability and deformation mechanisms of one-component, cementitious, flexible waterproofing membranes. Cement and Concrete Research, 136, 106140. https://doi.org/10.1016/j.cemconres.2020.106140.

[4] Waldvogel, M., Zurbriggen, R., Toropovs, N., Berger, A., & Herwegh, M. (2023). Distribution and evolution of (micro)strain and stresses in flexible, waterproofing membranes using digital image correlation and finite element modelling. Cement and Concre-

te Composites, 138, 104982. https://doi.org/10.1016/j.cemconcomp.2023.104982.
[5] Baskaran, B. A., Murty, B., & Wu, J. (2009). Calculating roof membrane deformation under simulated moderate wind uplift pressures. Engineering Structures, 31(3), 642–650. https://doi.org/10.1016/j.engstruct.2008.10.013.
[6] Darwish, Y., & ElGawady, M. (2023). Finite element analysis of TPO membrane-retrofitted metal roof system subjected to wind loads. Structures, 50, 330–346. https://doi.org/10.1016/j.istruc.2023.02.031.
[7] Azadvar, N., Zargaran, M., Rahimzadeh Rofooei, F., & Attari, N. K. A. (2021). Experimental comparison of cyclic behavior of RC columns strengthened with TRC and FRP. Bulletin of Earthquake Engineering, 19(7), 2941–2970. https://doi.org/10.1007/s10518-021-01092-2.
[8] Azadvar, N., Zargaran, M., & Attari, N. K. A. (2025). Numerical investigation of strengthening reinforced concrete columns with FRP in two directions under axial and cyclic loadings. European Journal of Environmental and Civil Engineering, 29(11), 2347–2368. https://doi.org/10.1080/19648189.2025.2484403.
[9] Zargaran, M., Attari, N. K. A., & Azadvar, N. (2025). Seismic behavior of infill and nonstructural masonry walls strengthened with textile reinforced mortar. Construction and Building Materials, 458, 139691. https://doi.org/10.1016/j.conbuildmat.2024.139691.
[10] EN 1990. Eurocode: Basis of Structural Design. European Committee for Standardization, Brussels.
[11] EN 1991-1-1. Eurocode 1: Actions on Structures - Part 1-1: General Actions - Densities, Self-weight, Imposed Loads for Buildings.
[12] EN 1991-1-3:2003+A1:2015. Eurocode 1: Actions on Structures - Part 1-3: General Actions - Snow Loads.
[13] EN 1991-1-4:2005+A1:2010 and EN 1991-1-5:2003. Eurocode 1: Actions on Structures - Wind Actions and Thermal Actions.
[14] EN 1998-1:2004+A1:2013. Eurocode 8: Design of Structures for Earthquake Resistance - Part 1: General Rules, Seismic Actions and Rules for Buildings.
[15] ASCE/SEI 7-22. Minimum Design Loads and Associated Criteria for Buildings and Other Structures. American Society of Civil Engineers, Reston, VA, 2022.
[16] ABAQUS User Documentation, 2024.

Authors:
Dr Narges Azadvar *– The University of Sheffield, School of Mechanical, Aerospace and Civil Engineering, Sheffield, UK.*
Dr Maurizio Guadagnini *– The University of Sheffield, School of Mechanical, Aerospace and Civil Engineering, Sheffield, UK. Department of Architecture, Construction Engineering and the Built Environment, Politecnico di Milano – polimi, Milan, Italy.*
William Jack Finley *– Roberts Group Company, Flint, Wales, UK.*
Professor Iman Hajirasouliha *– The University of Sheffield, School of Mechanical, Aerospace and Civil Engineering, Sheffield, UK.*

ACKNOWLEDGEMENTS

The authors acknowledge Roberts Group for providing the product information and experimental material data used in this study.

This project has received funding from the European Union research and innovation program under the Marie Skłodowska-Curie grant agreement (Acronym: STRENGTH, Entitled: Low-Carbon Geopolymer Textile Reinforced Concrete for Seismic Strengthening) No. 101207802. The authors would like to thank the European Union for their financial support.

NOVÝ BETON VE STARÉM ZDIVU? Z DĚJIN INOVACÍ.

NEW CONCRETE IN OLD MASONRY? FROM THE HISTORY OF INNOVATIONS.

Mgr. Lukáš Beran, Ph.D.

Abstrakt:
Využití moderních materiálů na bázi cementu při sanaci historických klenutých konstrukcí prošlo v průběhu dvacátého století pozoruhodným vývojem, který odráží nejen hromadění praktických zkušeností, ale také proměnu vnímání hodnot, jež pro nás tyto stavby představují.

Abstract:
The use of modern cement-based materials in the rehabilitation of historic vaulted structures underwent a remarkable evolution during the twentieth century, reflecting not only the accumulation of practical experience but also a shift in perceptions of the values these structures represent for us.

Key words: *masonry bridge; heritage protection; historical value; constructive conservation*

The repair of one of Europe's most historically significant bridges, in Regensburg, Bavaria, began in 2002 with the realization that *'...the serious rehabilitation errors of the 1960s had to be removed through painstaking, meticulous work. Repairs to the masonry using reinforced shotcrete and dense cement mortar increased the moisture load within the masonry and thereby caused further deterioration of the natural stone.'* [1] The reconstruction of the war-damaged spans of the Regensburg bridge, completed in 1967, in which *'blocks of green sandstone served merely as permanent formwork for the construction of reinforced-concrete arches',* [2] reflected a globally shared techno-optimism, but also the conviction that reconstruction of a heritage structure should primarily restore its external appearance.

In post-war Czechoslovakia, similar views underlay a whole series of inventive building interventions that helped preserve the very existence of many important structures—albeit, from today's perspective, at too high a cost. A key figure of this period was the structural engineer Bedřich Hacar (1893–1963). [3] His papers, held by the CTU Archive in Prague, include a typescript draft of a lecture delivered on 23 May 1950 at the College of Civil Engineering of the Czech Technical University in Prague, with the telling title *'Cement, the Principal Means for the Reconstruction of Monumental Buildings'.* Hacar focused above all on masonry grouting, the strengthening of vaults on the extrados by reinforced-concrete shells, but also on *'replacing missing parts of old masonry structures with new structures of the same form, but made of reinforced concrete'.* [4]

As for grouting, the technique was by no means new at the time: as early as 1835, Louis Alexis Beaudemoulin used it to stabilize—albeit temporarily—the piers of the then century-old bridge over the Loire in Tours. [5] Yet the technology entered heritage conservation only later from hydraulic engineering and from tunnel construction and maintenance. The Berlin firm August Wolfsholz, which used the method in these fields, [6] had advertised the *'Sanierung einsturzdrohender Baudenkmäler'* [rehabilitation of monuments at risk of collapse] since 1914, and its first project in the territory of present-day Czechia was probably the stabilization of the north tower of the parish church of St James in Jihlava in 1922. [7]

Strengthening vaults by applying a sprayed and reinforced concrete layer to their extrados likewise has a longer history. It was made possible by the shotcreting process, developed in the 1920s on the basis of earlier patents by the Dresden engineer Josef von Vaß, again initially for tunnel construction but also for stabilizing the walls of deep mine shafts. [8] One documented example is the rescue of the vaults of St George's Church in Cologne by shotcreting in 1928. [9] With the development of reinforced-concrete shell structures, the reinforcement of such layers came to be designed according to membrane theory, and they were therefore commonly described as 'extrados shells', although they were not necessarily self-supporting structures and could instead act compositely with the original vault through anchors. [10] In many cases, however, they assumed the load-bearing function entirely. One example is the shells from which, in 1950, the Gothic vaults of the church chancel and the cloister of the Emmaus Monastery in Prague were suspended; Bedřich Hacar worked on its post-war reconstruction together with the architect Bedřich Stefan. [11] Hacar had been developing the first reinforced-concrete shells in Czechoslovakia at the future Klokner Institute since 1941, originally for industrial buildings. [12] He replaced the destroyed vaults of the church's central

nave with structures only 5 cm thick, shaped in a Gothic manner and fitted on the soffit with prefabricated ribs. Similarly, in collaboration with the architect Pavel Janák, Hacar designed a shell completed in 1947 as a formal analogue of the Renaissance vault of the Ball Game Hall at Prague Castle, exactly 330 years after that vault had collapsed. Today, these interventions can be understood as specific manifestations of modern architecture responding to wartime destruction, yet they also had a profound influence on heritage-conservation practice.

'Until recently, it was customary in heritage conservation to restore old monuments using traditional methods and materials, and conservation professionals often resisted modern materials, regarding them as foreign elements in the body of the monument. (...) The old methods are highly labour-intensive, restoration is protracted and productivity is low. These shortcomings are particularly pronounced in cases where structural equilibrium has been disturbed, the number of which has been rapidly increasing as a result of inadequate maintenance in recent decades.' [13] This was how Zdeněk Fuka, a former assistant to Bedřich Hacar during rescue works on monuments affected by the construction of the Orlík Dam, summarized the situation in 1967. In doing so, he employed a metric that was crucial to Czechoslovakia's centrally planned economy: labour intensity, or, in later terminology, 'labour productivity'. As another prominent structural engineer specializing in historic monuments recalled, the spread of these methods must also be attributed to the initiative of enterprises originally specialized in mineral exploration which, after mining activity declined, were assigned by the state to carry out 'monument sanation'—first in cellars within historic urban fabric, and later on far more complex projects. [14] At project level, however, this led to the *'autonomization and prioritization of structural stabilization'*[15] and subsequently to the widespread, and often unnecessary, use of masonry grouting, strengthening with reinforced-concrete ring beams, and the reinforcement of vaults by a layer of reinforced shotcrete. The destructive consequences of moisture accumulation in buildings stabilized with cement and concrete soon became apparent in practice. At the same time, however, Czechoslovak conservationists participated in the international formulation of the fundamental theoretical principles of their field, summarized at the time in the ICOMOS Venice Charter. *'One of the principal tenets of modern heritage conservation is equal protection of both the architectural style and the construction of a building; a complete alteration of the construction through grouting must therefore be approached with great caution and employed only where no other option remains and where we have decided to sacrifice the authenticity of the construction and content ourselves with preserving its form. The monument then becomes a mock-up...'* [16]

The development of structural mechanics in the post-war period also brought a renewed interest in its history—and thus a deeper understanding of the principles by which historic structures were designed and how they function structurally. Stephen Timoshenko's (1878–1972) seminal work of 1953 summarized the historical development of advanced theory, [17] while the history of its practical applications—that is, the relationships between science and traditional know-how—remains a rapidly developing field, whose beginnings may be associated above all with the work of Edoardo Benvenuto (1940–1998). [18] For millennia, the 'rules of art'—empirically tested rules that used simple equations to determine the span, geometric form and thickness of vaults as well as the dimensions of their supports—formed the basis for the design of bridge structures even at a time when such designs could already be verified by structural calculation: from the seventeenth century on the basis of strength od solids theory, and in the second half of the nineteenth century by new methods based on elasticity theory or graphical statics. [19] The advent of new materials—iron and concrete—also gave rise to the concept of the 'structure' as the load-bearing component of a building, independent of its architecture and governed by its own rules and design methods. In the twentieth century this component also became physically separated from the architectural envelope, just as the teaching of civil engineering became separated from architecture in schools. *'Historical constructions go outside the structural conceptions of this century's architects and engineers who, proud of the new forms of structural engineering and new materials, view historical buildings as artificial obsolete forms to be reinterpreted according to the analytical models and static plans of the new theory and to be restored through the use of more or less calculated extension and consolidation work which alters the ancient construction conception of these buildings for the sake of guaranteeing an undefined and perhaps presumptious degree of safety.'* [20] At the very end of the twentieth century, Mariangela Bellomo and Salvatore D'Agostino formulated approaches to the protection of historic structures based on their original construction principles, later characterized as 'structural conservation'—surely not by chance in Italy, a country exceptionally rich in such monuments—first as guidelines for safeguarding them against earthquakes [21] and, more recently, as a general methodological handbook. [22] They identify the following fundamental principles: *'Respect for the ancient constructive conception; Homogeneity of materials and techniques (i. e. not to alter the mechanical and physical-chemical behaviour of the construction, not to modify the original distribution of the states of stress, and not to induce phenomena of deterioration owing to incompatibility between the materials employed); Principle of minimal intervention, to be programmed in a spirit of improvement and possible reversibility; Programmed maintenance.'* In this way, engineers-historians reformulated, thoroughly and independently, principles that heritage-conservation specialists had already reached in the 1960s.

Can these principles, however, be applied consistently to monuments whose significance is primarily structural—that is, to bridges? The principal reason for their alteration in the past, as today, has been the growth of traffic intensity, creating a need to increase load-bearing capacity or widen the bridge deck—not the safety of the structure itself. [23] Strengthening vaults from the extrados with a reinforced-concrete layer had been common in Czechoslovakia since the 1930s, both on road bridges, such as the stone bridge at Poniklá dating from 1853, [24] or the much older Pitr's Bridge in Rajhrad (which at that time was also provided with a projecting reinforced-concrete deck), [25] and on railway bridges, such as the 1848 'Red Bridge' near Bratislava, where in 1935 reinforced-concrete vaults took over two-thirds

of the load carried by the original brick vaults. [26] The issue may ultimately be one of degree: at what point does a new structure still strengthen the original vault, and at what point is the result instead a reinforced-concrete vault with masonry facing? Similar questions arise from the common practice of replacing, and sometimes widening, a bridge deck originally paved directly over the vault fill with a reinforced-concrete slab—a method applied almost universally in Czechoslovakia and Czechia from the mid-twentieth century to the present. Early examples include the alteration of the floodplain bridge at Předměřice nad Jizerou in 1939–1940 and the bridge in Žďár nad Sázavou in 1947; the 1985 reconstruction of the so-called Cheb Bridge in Karlovy Vary is another well-known case. The harmful effects of preventing the upward passage of moisture and water vapour through the bridge structure are therefore well known. [27] Nevertheless, bridges at Kobylince (2003) and Verměřovice (2008) were recently rebuilt in a similar way, and even the reconstruction of as heritage listed Prague's Negrelli Viaduct (2017–2019) involved a wide reinforced-concrete load-distribution slab. [28]

[1] SWACZYNA, Alfons. Kamenný most v Regensburgu: zachování evropské kulturní památky. In: *Oprava Karlova mostu: veřejný technický seminář* 13. dubna 2004. Praha: ŠEL 2004, pp. 61–64. ISBN 80-86426-16-5.

[2] EGERMANN, Ralph. Museumsstück oder Verkehrsbauwerk – Aspekte zur Instandsetzung der Steinernen Brücke in Regensburg, *Mauerwerk* 2020, 24 (1), pp. 57–65. ISSN: 1437-1022, DOI: 10.1002/dama.201910029

[3] VALENTA, Oldřich. 70 let akademika Bedřicha Hacara, *Stavebnicky časopis* 1963, 11 (5), pp. 297–312.

[4] Archive of the Czech Technical University in Prague, collection Bedřich Hacar, Prof. Ing. Dr., box no. 18. The final text was later published as HACAR, Bedřich. Rekonstrukce stavebních památek, *Město* 1950, 12 (4), pp. 181–195.

[5] BEAUDEMOULIN, Louis Alexis. Mémoire sur les divers mouvements du pont de Tours... *Annales des ponts et chaussées* no. 380, 1836, vol. 2, pp. 86–133 and plates CLXXIII, CLXXIV, and CLXXV.

[6] BERGS, Werner. Von Preßzementbau. *Prometheus* 1915, 26 (1336), pp. 565–568 and (1937), pp. 584–586.

[7] MÍKA, Ludvík. Zajišťování jižní věže farního chrámu sv. Jakuba v Jihlavě, *Zprávy veřejné služby technické* 1925, 7 (4), pp. 106–110; cf. NEJEDLÝ, Vratislav. Příspěvek k poznání počátků využívání moderních technologií v oblasti památkové péče. *Památky a příroda* 1984, 9 (7), pp. 385–391.

[8] SZILARD, Adalbert. *Das Torkretverfahren und seine technischen Probleme*. Berlin: J. Springer 1925.

[9] SCHORN, Wilhelm. Die Sicherung der katholischen Pfarrkirche St. Georg in Köln. *Jahrbuch der rheinischen Denkmalpflege* 1930, 23 (5/6), pp. 120–127.

[10] PAVLÍK, Milan. *Regenerace historických budov, sídel a krajiny, ochrana památek*. Praha: ČVUT 1998, p. 111. ISBN 80-01-01797-4.

[11] HACAR, Bedřich. Obnova kostela a kláštera Emauzského, *Ochrana památek: Věstník Klubu Za starou Prahu a jeho odborů* 1952, 27 (5), pp. 33–34.

[12] BERAN, Lukáš. Dialektika konstrukce: K podstatě průmyslové architektury v Československu druhé poloviny 20. století, in: ZIKMUND, Jan (ed) – LEHKOŽIOVÁ, Irena (ed), *Architektura produkce: Průmysl, stát a společnost v Československu 1939–1992*. Praha: ČVUT 2026. ISBN 978-80-01-07553-1 (in print).

[13] FUKA, Zdeněk. Novodobé způsoby sanace památkového zdiva sanačními maltami, in: *Technické metody v památkové péči: referáty z kolokvia v Kutné Hoře, říjen 1967*. Praha: Státní ústav památkové péče a ochrany přírody 1968, pp. 5–31. Fuka's introduction to an otherwise predominantly technical paper also contains a remarkable reflection: *'Fears that "prostheses of iron and concrete" will one day protrude above a ruin and disfigure these picturesque remains are illogical, because by the time this happens, these strengthening elements will themselves have become monuments, and our descendants will regard them in the same way as we today assess the primitive stabilizing structures of past centuries.'* (p. 8)

[14] VINAŘ, Jan. Cement a beton při statickém zajištění a konzervaci památek, in: *Beton a památková péče*. Praha: Axis, 2015, pp. 33–39. ISBN 978-80-904081-7-3.

[15] ŠTULC, Josef. K ožívání romantických koncepcí a puristických metod při sanaci a komplexní obnově stavební památek, *Památky a příroda* 1984, 9 (3), pp. 129–142. ISSN 0139-9853.

[16] ŠTORM, Břetislav. *Základy péče o stavební památky*. Praha: Státní ústav památkové péče a ochrany přírody 1965, p. 24. Cf. *The Venice Charter of 1964* (the International Charter for the Conservation and Restoration of Monuments and Sites), Article 10: *'Where traditional techniques prove inadequate, the consolidation of a monument can be achieved by the use of any modern technique for conservation and construction, the efficacy of which has been shown by scientific data and proved by experience.'* https://www.icomos.org/images/DOCUMENTS/Charters/venice_e.pdf [Accessed 2026-10-20]

[17] TIMOSHENKO, Stephen. *History of Strength of Materials.* 1953 New York: McGraw-Hill. Cf. KURRER, Karl-Eugen. *The History of the Theory of Structures: From Arch Analysis to Computational Mechanics*. Berlin: Ernst & Sohn 2008, https://ebookcentral.proquest.com/lib/natl-ebooks/detail.action?docID=482146 [Accessed 2026-10-20]

[18] BENVENUTO, Edoardo. La Scienza delle costruzioni e il suo sviluppo storico, Firenze: Sansoni 1981; English ed.: *An Introduction to the History of Structural Mechanics.* New York: Springer 1991. ISBN 978-1-4612-7751-4.

[19] CORRADI, Massimo. Empirial methods for the construction of masonry arch bridges in the 19th century. In: SINOPOLI, Anna (ed).

Arch bridges: proceedings of the 2nd International Arch Bridge Conference, Venice, Italy, 6–9 October 1998: history, analysis, assessment, maintenance and repair. Rotterdam: Balkema 1998, pp. 25–36. ISBN 90-5809-012-4.
[20] BELLOMO, Mariangela – D'AGOSTINO, Salvatore. Construction conception and structural conservation of masonry arch bridges. Ibidem, pp. 535–339.
[21] BELLOMO, Mariangela – D'AGOSTINO, Salvatore. Improvements as a criterion for the antiseismic safeguarding and structural conservation of historical sites: methodology and examples. In: *12th World Conference on Earthquake Engineering* (12WCEE), 1999. https://www.semanticscholar.org, Corpus ID: 195752051. [Accessed 2026-10-20]
[22] D'AGOSTINO, Salvatore. *Conservation and Restoration of Built Heritage: A History of Conservation Culture and its More Recent Developments.* 2021, CRC Press. https://doi.org/10.1201/9781003160960 [Accessed 2026-10-20]
[23] PROSKE, Dirk – VAN GELDER, Pieter. *Safety of Historical Stone Arch Bridges.* Springer 2009. ISBN 978-3-540-77616-1.
[24] PANÁČEK, Michal – JAKUBEC, Pavel – ŘEŘICHA, Petr – FAJMAN, Petr. Historie a záchrana kamenného klenbového mostu v Poniklé na řece Jizeře. *Zprávy památkové péče* 2025, 85(2), pp. 130–144.
[25] ~, Rajhrad. *Zprávy památkové péče 1938*, 2 (1), p. 14.
[26] LAUŠNER, František. Přestavba železničního viaduktu 'Červený most' u Bratislavy. *Zprávy veřejné služby technické* 1936, 18(2), pp. 34–42.
[27] VINAŘ, Jan. *Metodika oprav nosných konstrukcí památkově chráněných objektů: Zajištění statické funkce při zachování autenticity.* Praha: NPÚ 2022, p. 105. ISBN 978-80-7480-156-3.
[28] ČERNÁ VYDROVÁ, Linda – PELEŠKOVÁ, Michaela. Rekonstrukce Negrelliho viaduktu v Praze. *Beton* TKS 2018 (4), pp. 3–10. ISSN 1213-3116.

Mgr. Lukáš Beran, Ph.D.,
Faculty of Architecture –
Czech Technical University in Prague,
lukas.beran@fa.cvut.cz

This paper is an output of the project Technologies and procedures for the protection of historic masonry bridges of the 19th and early 20th centuries (DH23P03OVV024), funded under NAKI III, the applied research and development programme of the Ministry of Culture of the Czech Republic.

DECONTAMINATION AND CLEANING OF INTERIOR NATURAL STONE SURFACES AT NOTRE-DAME DE PARIS AFTER THE 2019 FIRE

DEKONTAMINACE A ČIŠTĚNÍ VNITŘNÍCH POVRCHŮ Z PŘÍRODNÍHO KAMENE V KATEDRÁLE NOTRE-DAME V PAŘÍŽI PO POŽÁRU V ROCE 2019

Dipl.-Ing. Jens Engel, Remmers GmbH, Bernhard-Remmers-Str. 13, 49624 Löningen, Germany

Abstract
After the fire of 15-16 April 2019, the interior of Notre-Dame de Paris was affected not only by soot, dust and construction debris, but also by lead-containing deposits released from the historic roof covering. The restoration therefore required a cleaning strategy that could remove contamination from limestone, sculptural elements and complex architectural surfaces while limiting dust generation, water input and secondary emissions in the cathedral interior. This paper describes the evaluation of cleaning methods and the practical implementation of a natural-latex peel-off cleaning system on interior stone surfaces. Test areas were assessed with regard to visual cleaning performance, residual lead load, handling time, changes in water absorption and potential salt-related damage. Based on the test results, a specially formulated Arte Mundit peel-off paste was selected. The system forms an elastic film after drying, binds removed particles within the film and enables residue control by UV illumination. The case demonstrates how conservation requirements, occupational safety and large-scale site logistics can be combined in the remediation of a highly significant monument.

Abstrakt
Po požáru ve dnech 15. a 16. dubna 2019 byl interiér katedrály Notre-Dame de Paris zasažen nejen sazemi, prachem a stavebním odpadem, ale také usazeninami obsahujícími olovo, které se uvolnily z historické střešní krytiny. Restaurování proto vyžadovalo strategii čištění, která by dokázala odstranit znečištění z vápence, sochařských prvků a složitých architektonických povrchů a zároveň omezila tvorbu prachu, spotřebu vody a sekundární emise v interiéru katedrály. Tento článek popisuje vyhodnocení metod čištění a praktické použití čisticího systému na bázi přírodního latexu s odlupovací pastou na kamenných površích v interiéru. Testované plochy byly posuzovány z hlediska vizuální účinnosti čištění, zbytkového obsahu olova, doby zpracování, změn ve vstřebávání vody a potenciálního poškození způsobeného solemi. Na základě výsledků testů byla vybrána speciálně vyvinutá odlupovací pasta Arte Mundit. Tento systém po zaschnutí vytváří pružný film, který v sobě váže odstraněné částice a umožňuje kontrolu zbytků pomocí UV osvětlení. Tento případ ukazuje, jak lze při sanaci vysoce významné památky skloubit požadavky na konzervaci, bezpečnost práce a logistiku rozsáhlého staveniště.

Key words: *Notre-Dame de Paris; lead decontamination; natural stone cleaning; latex peel-off paste; cultural heritage conservation; Arte Mundit*
Klíčová slova: *Notre-Dame de Paris; odstraňování olova; čištění přírodního kamene; latexová odlupovací pasta; ochrana kulturního dědictví; Arte Mundit*

1. INTRODUCTION

During the night of 15 to 16 April 2019, parts of one of the most important historic buildings in Europe and one of the defining landmarks of France were destroyed by fire: the cathedral of Notre-Dame de Paris. After the outbreak of the fire, the Paris fire brigade succeeded within approximately four hours in largely confining the fire to the timber roof structure. Nevertheless, parts of the roof and of the vaults collapsed into the church interior.

The subsequent restoration presented an exceptional conservation challenge. The objective was not only to secure and restore the damaged building fabric, but also to remove contamination that had been dispersed throughout the interior during and after the fire. This concerned the natural stone surfaces of walls, piers, vaults, sculptural elements and floor areas, many of which are historically significant, highly textured and partially heat-damaged.

This contribution focuses on the clea-



Figure 1: *Notre-Dame de Paris. The cathedral has been a UNESCO World Heritage site since 1991 and is an outstanding example of Gothic architecture. Photo: Remmers.*

ning and decontamination of interior natural stone surfaces for which Remmers GmbH, Löningen, supplied materials. The emphasis is placed on the test programme, the selection of a latex-based peel-off cleaning paste, the practical execution of the work and the quality assurance measures used on site.

2. CONTAMINATION CHALLENGE AFTER THE FIRE

Depending on the source, up to approximately 460 tonnes of lead roofing are assumed to have melted and partly vaporised during the fire. The resulting lead dust was distributed in the surroundings and inside the cathedral. Metallic lead vaporises perceptibly from about 550 °C. In dust or vapour form, it oxidises in air to colloidal lead oxide (PbO). This so-called lead fume consists of lead oxide particles that can adhere to a wide variety of surfaces.

Lead and inorganic lead compounds are associated with numerous adverse effects on human health. The effects described in occupational-health literature include symptoms such as general fatigue, weakness, loss of appetite, irritability, headache, dizziness, constipation, abdominal colic, nausea or vomiting, and paralysis of peripheral motor nerves. In cases of massive exposure, encephalopathy may occur. Effects on blood formation, the kidneys, the nervous system, reproductive capacity and the cardiovascular system are also described.

Philippe Villeneuve, the chief architect responsible for historic monuments in France, requested that the Laboratoire de Recherche des Monuments Historiques (LRMH), the central laboratory of French heritage conservation, develop a concept for cleaning and decontaminating the cathedral. This was based on the justified concern that the lead cloud released by the fire had contaminated specific areas. The concern was reinforced by the fact that, during sorting of the debris that had fallen to the floor, many kilogrammes of lead were found every day, ranging from millimetre-sized particles to pieces several decimetres in size.

Quantitative analyses of wipe samples taken from the cathedral paving in accordance with NF X 46-030 produced values well above 100,000 micrograms per square metre. The French permissible limit value of 1,000 micrograms per square metre was therefore exceeded clearly in almost the entire cathedral, at least on floor surfaces.

In July 2019, work that had already begun at Notre-Dame had to be interrupted because the safety rules for workers were not sufficient. In the interim, an extremely strict safety protocol applied to everyone involved on the site. Clothing had to remain on site for decontamination every time workers and visitors left the work area, and every person leaving the site had to shower.

3. TEST AREAS AND ASSESSMENT METHODOLOGY

The Saint-Eloi Chapel, located on the north side of the nave and featuring no painted decoration, was selected together with two further areas and scaffolded in order to carry out cleaning and lead-removal tests. In this chapel, tests could be performed on different substrates such as stained glass, metal, wood and stone under comparable exposure conditions. The present paper discusses in detail only the tests and subsequent cleaning works carried out on stone.

In its preliminary investigations, the LRMH did not concentrate solely on the visual cleaning effect of possible methods and materials and their residue-free removal. Particular attention was also paid to the extent to which lead-containing dusts could be removed from surfaces without being released again into the environment or into the interior of the monument.

In all test areas, one surface was left completely untreated as a reference. All further test areas were first vacuum-cleaned using equipment fitted with special filters in order to remove loose components in a simple manner. One of these vacuum-cleaned areas was not treated further and thus served as an additional reference.

Injection/extraction cleaning

In this method, the cleaning medium, in this case water without further additives, is sprayed under pressure onto the surface by means of a spray-suction nozzle and is immediately extracted together with the dirt. Compared with cleaning using simple high-pressure washers, the stone absorbs comparatively little water.

Latex-based peel-off pastes

This type of product has proved effective over the past two decades for systematic cleaning of large interior areas in historic buildings. The decisive advantages are that practically no water is used, no dust is generated and the dirt particles removed from the surface are bound in the cleaning film. They are therefore not emitted into the room and can be disposed of together with the cleaning product in a controlled manner. At Notre-Dame, the pastes were applied using different tools and methods, in-

cluding brushes, spatulas and airless spraying. After approximately one day, the paste had dried and polymerised to form a highly elastic film which, depending on its thickness, could be peeled from the surface in large coherent pieces. All test areas treated with peel-off cleaners were subsequently cleaned with a damp sponge, because a fine dust can remain on the substrate after film removal, especially when the paste contains complexing chemical auxiliaries.

Poultices

Six different poultices were also applied to floor areas and vault zones, using different tools and procedures. These poultices harden merely by drying, with a certain internal bonding of their constituents, so that they can subsequently be removed from the surface in larger pieces. In some cases they lose adhesion to the substrate already during drying and can then be removed easily and without residues. A damp-sponge after-cleaning step was also carried out after cleaning with poultices.

The remaining lead contamination on the test areas was subsequently assessed by two principal methods, supplemented by conservation-specific evaluations of handling, effectiveness, water absorption and salt-related damage potential.

ICP-AAS on wipes

This method, applied according to the approach described in NF X 46-032, was originally developed for the quantification of lead in dust during post-control inspections of work in the presence of lead. Surface-adhering dust is collected with moistened wipes and analysed quantitatively. After cleaning, the value had to be below 1,000 micrograms per square metre. A comparable workflow is provided by Remmers and the Bernhard Remmers Institute for Analytics under the name LEAD-Box.

Portable X-ray fluorescence

Portable X-ray fluorescence, referred to in France as FLUOX, is frequently used on historic monuments. One disadvantage is that the generated X-rays penetrate to different depths depending on the type of material and the inhomogeneity of the substrate. The interpretation of results is therefore limited. Measurements were consequently carried out not only directly on the substrate, but also on surface dust samples removed with adhesive tape. For sampling, a 2 x 5 centimetre strip of double-sided Scotch 3M adhesive tape with an extra-strong, smooth surface is applied to the surface and pulled off. This sampling method was used systematically on both the uncleaned substrate and the respective cleaned test surfaces.

Handling of cleaning methods

Only time values measured on the object were evaluated. For each cleaning method, the pre-wetting time, application time, dwell time, removal time of the cleaning products and duration of after-cleaning were recorded.

Cleaning effectiveness

Effectiveness was assessed by measuring the colour change of the substrate and by determining the residual contamination rate. For the latter, measurements were carried out by 3D digital microscopy and by scanning electron microscopy with energy-dispersive X-ray spectroscopy, both directly on the substrate and on adhesive-tape surface dust samples.

Change in water absorption

Water absorption was measured by a sponge test. A defined sponge is saturated with a defined quantity of water and pressed against the test surface with a plastic plate. After a defined contact time, the sponge is weighed again. The difference in mass indicates how much water has been absorbed by the surface. Although the method is not standardised, it is established through scientific studies and its use in a number of conservation projects.

Medium-term damage potential

The medium-term damage potential was assessed on scratch samples by determining the content of soluble salts in accordance with EN 16455. The amount and type of salts indicate whether salts were formed or mobilised by the cleaning process.

4. SELECTED CLEANING SYSTEM

After evaluation of all results, the decision was made in favour of one of the latex-based peel-off pastes, specifically one of the tested Arte Mundit types. The selected material was a specially formulated aqueous dispersion based on natural rubber. Natural rubber dispersions are usually stabilised with ammonia; the Arte Mundit dispersion used in this project was formulated without ammonia, making it possible to use the product without extraction of ammonia emissions.



Figure 2: *Arte Mundit peel-off paste on site at Notre-Dame de Paris. Photo: Remmers.*



Figure 3: *Airless equipment during application of the peel-off paste. Photo: Remmers.*

When the product is applied to the wall surface, water evaporates during drying and the dispersed polymer crosslinks to form a firm but very elastic film. The product is designed for use in historic interiors where the room climate cannot always be controlled. Its formulation therefore permits use over a broad climatic range. Under normal humidity conditions, it can be applied without difficulty at material, ambient and substrate temperatures between +5 °C and +30 °C.

A particular innovation in Arte Mundit is the addition of a UV-reflective pigment. At Notre-Dame, this allowed the cleaned wall surfaces to be inspected under black light in order to identify any remaining latex residues. This was an important quality-assurance step, especially in areas with complex geometry.

5. EXECUTION OF THE CLEANING WORKS

The cleaning covered approximately 70,000 square metres of interior surface. This included walls, sculptures, vaults, floor surfaces and even areas with wall paintings. Handling heat-damaged limestone was particularly sensitive, because some stone had lost strength due to the extreme temperatures. The procedure had to ensure that lead contamination was removed while preserving the historic substance of the building.

Another difficulty, although encountered only to a limited extent, was high moisture content in the natural stone, caused by firefighting water and partly by rainwater ingress. If the substrate is too wet, sufficient adhesion between the cleaning system and the substrate does not develop, and the peel-off process cannot be effective. These areas had to be dried before cleaning could proceed.

The cleaning work was carried out by three companies: H. Chevalier, Tollis and Atelier Bouvier. One company was responsible for large flat areas such as walls and piers, one for sculptural elements such as capitals, and one for the remaining detailed areas. The cleaning of the walls, the largest surface area, was performed by the restoration contractor H. Chevalier.

The procedure consisted of the following steps:

- Sensitive areas such as gilding, polished metals, painted surfaces and adjacent zones were covered with PE film or non-woven fabric.
- The soiled masonry surfaces were then vacuum-cleaned in order to remove coarse dirt particles.
- Before application, the latex paste was thoroughly homogenised to ensure a uniform consistency.
- Application was largely mechanical, using airless spraying equipment. Only particularly difficult-to-access areas or reworking zones were treated manually with brushes, lambskin rollers or spatulas. The paste was applied evenly over the entire surface, carefully filling recesses and contours. Consumption was approximately 1 kilogram per square metre on flat wall areas and up to 3 kilograms per square metre on figurative or carved surfaces.
- The crosslinked film was generally peeled off on the day after application. Samples of the removed material were analysed for lead content, and the films were packed in big bags. Depending on lead content, the big bags were sent for incineration or landfill disposal.
- Finally, wall surfaces in some areas were wiped with a slightly damp sponge to remove residual dust. This step is customary in particular for pastes containing complexing agents, since film formation may occur faster than the complexation process.
- All wall surfaces were inspected with a black-light lamp in order to detect any remaining peel-off cleaner residues and to remove them where necessary. Such residues are typically found only in difficult-to-access areas, for example in niches behind engaged columns.



Figure 4: *Column coated with Arte Mundit after drying and crosslinking of the natural latex. Photo: Remmers.*



Figure 5: *Removed latex film. Dirt adhering to the back of the peel-off film reproduces the masonry structure. Photo: Remmers.*

6. CONCLUSION AND OUTLOOK

During the 2019 fire at Notre-Dame de Paris, the roof structure above the nave and transept was destroyed, and lead contamination was deposited on interior surfaces throughout the cathedral.



Figure 6: *Packaging of removed latex films in big bags marked Pb for lead-containing waste. Photo: Remmers.*



Figure 7: *Inspection of cleaned wall surfaces under black light to identify and remove remaining peel-off residues. Photo: Remmers.*

Following extensive preliminary investigations, this contamination was removed from natural stone surfaces using a natural-latex-based peel-off cleaning system. The cleaning principle is based on the mechanical removal of surface deposits and, where relevant, chemical removal through chelation of specific compounds.

Before its use at Notre-Dame, the method had already been applied in numerous historic buildings for the cleaning of interior wall surfaces and for the removal of fire residues in secular buildings in Germany and other European countries. The Notre-Dame project demonstrates how a conservation-grade cleaning system can be scaled to a highly complex monument while addressing health protection, waste management and residue control.

At the end of 2024, Notre-Dame de Paris was reopened after successful restoration of the interior. The experience gained in the project is relevant for future interventions on contaminated historic interiors, especially where dust binding, low water input, reversibility of the cleaning medium and reliable quality assurance are decisive requirements.

REFERENCES

[1] New York Times. Lead contamination after the Notre-Dame fire. Available online: https://www.nytimes.com/interactive/2019/09/14/world/europe/notre-dame-fire-lead.html (accessed on 24 October 2025).

[2] Deutsche Gesellschaft für Arbeitsmedizin und Umweltmedizin (DGAUM). Prävention und Früherkennung arbeitsbedingter Gesundheitsgefährdungen bei Tätigkeiten unter Einwirkung von Blei und seinen anorganischen Verbindungen. S1 guideline.

[3] RND. Bleiverschmutzung: Arbeiten an Notre-Dame werden fortgesetzt. Available online: https://www.rnd.de/panorama/bleiverschmutzung-arbeiten-an-notre-dame-werden-fortgesetzt-H3XGIRH4V3IDVSJG7UOKKVN7FQ.html (accessed on 24 October 2025).

[4] Laboratoire de Recherche des Monuments Historiques / project communication on cleaning tests at Notre-Dame de Paris, personal communication.

[5] Remmers GmbH. LEAD-Box test set. Available online: https://www.remmers.com/de/werkzeuge/test-sets/lead-box/p/000000000000496901 (accessed on 24 October 2025).

[6] Drdacky, M.; Slizkova, Z. Sampling and assessment of surface dust on historic materials using adhesive tape. 2015.

[7] Vandevoorde, D.; Cnudde, V.; Dewanckele, J.; Brabant, L.; de Bouw, M.; Meynen, V.; Verhaeven, E. Contact sponge method: Performance of a promising tool for measuring the initial water absorption. Journal of Cultural Heritage 2009.

[8] EN 16455: Conservation of cultural heritage - Extraction and determination of soluble salts in natural stone and related materials used in and from cultural heritage.



Figure 8: *Interior of Notre-Dame de Paris after reopening. Photo: Remmers.*

Authors

Dipl.-Ing. Jens Engel – Remmers GmbH, Bernhard-Remmers-Str. 13, 49624 Löningen, Germany. Head of Product Management Construction.

Acknowledgements

The author thanks the project partners, conservation specialists and restoration companies involved in the cleaning works at Notre-Dame de Paris. Photographs: Remmers.

THERMAL COMPATIBILITY OF REPAIR MORTARS WITH STONE AND BRICK SUBSTRATES

HODNOCENÍ TEPLOTNÍ KOMPATIBILITY OPRAVNÝCH MALT S KAMENNÝM A CIHELNÝM PODKLADEM

*NÁHUNKOVÁ Pavla[1] *, FRANKEOVÁ Dita[1], MÁCOVÁ[1] Petra and KUNECKÝ[2] Jiří*

Abstract
Thermal compatibility represents an important criterion in the selection of repair mortars for historic masonry. This study evaluates six mortar formulations based on natural hydraulic lime, Roman cement, white Portland cement, and their blends, in relation to selected stone and brick substrates. The apparent coefficient of linear thermal expansion (CTE) was determined using a push-rod dilatometer in the range of 25–80 °C. The CTE mismatch between mortar and substrate was assessed together with the Young's modulus obtained from bending tests, allowing the influence of both thermal strain and material stiffness to be considered. This combined approach provides a basis for the qualitative assessment of potential thermo-mechanical mismatch between repair mortars and masonry substrates.

Abstrakt
Teplotní kompatibilita představuje významné kritérium při výběru opravných malt pro historické zdivo. Předložená studie se zabývá hodnocením šesti malt na bázi přírodního hydraulického vápna, románského cementu, bílého portlandského cementu a jejich směsí ve vztahu k vybraným kamenným a cihelným podkladovým materiálům. Pomocí tyčové dilatometrie byl v teplotním rozmezí 25–80 °C stanoven zdánlivý součinitel délkové teplotní roztažnosti (CTE). Rozdíly v hodnotách CTE mezi maltami a podkladovými materiály byly hodnoceny ve spojení s Youngovým modulem pružnosti stanoveným ze zkoušek v ohybu. Společné posouzení těchto charakteristik umožňuje zohlednit rozdíly v teplotním přetvoření i tuhosti jednotlivých materiálů a vytváří základ pro kvalitativní hodnocení potenciálního termomechanického nesouladu mezi opravnou maltou a podkladem.

Key words: *historic masonry; repair mortars;thermal expansion, Young's modulus, thermo-mechanical compatibility.*
Klíčová slova: *historické zdivo; opravné malty; teplotní roztažnost; Youngův modul pružnosti; termomechanická kompatibilita.*

1. INTRODUCTION

Historic masonry bridges combine stone or brick masonry with mortars that may differ substantially in their mechanical, hygric, and thermal properties. Throughout their service life, they are exposed to repeated environmental loading, including fluctuations in temperature and moisture. The selection of a suitable repointing mortar is therefore challenging, as incompatible repairs may contribute to cracking, debonding, and deterioration of the adjacent substrate. Consequently, mortar performance should be assessed in relation to the specific masonry substrate.

Compatibility is commonly discussed in terms of mechanical strength, porosity, moisture transport, and durability [1, 2], whereas thermo-mechanical compatibility has received less attention than mechanical and hygric performance. Differences in the coefficients of thermal expansion of the mortar and substrate produce differential free thermal strains. When these strains are restrained by the interaction between the two materials, stresses may develop within the repair system and at the mortar-substrate interface. Numerical modelling has shown that the resulting stress state depends on the CTE mismatch, the Young's moduli of both materials, the temperature change or gradient, and the degree of deformation restraint [3].

The thermal and mechanical properties of mortars may also evolve with age as a consequence of continued hydration, carbonation, and associated microstructural changes, with the relative importance of these processes depending on the binder system [4, 5]. This is relevant to mortars based on natural hydraulic lime, Roman cement, white Portland cement, and their blends. However, the combined age-dependent evolution of thermal expansion and stiffness, particularly in relation to masonry substrates with contrasting properties, has received comparatively limited attention [3–5].

2. MATERIALS AND METHODS

Six experimentally prepared repointing mortars designed for historic masonry bridges were evaluated. The mortar compositions were selected to represent binder systems commonly used in conservation practice. The binders comprised natural hydraulic lime (M1, Calcidur Otterbein); natural hydraulic lime-Ro-

man cement blends at volumetric ratios of 1:1 (M2) and 3:1 (M3); a natural hydraulic lime-white Portland cement blend (1:1 by volume, M4); Roman cement (M5; Vicat); and white Portland cement (M6; HET). For all formulations, the binder-to-aggregate ratio was fixed at 1:2 by volume.

The mortar mixtures were prepared according to ČSN EN 1015-2. The water content was adjusted to obtain a flow diameter of 120–130 mm, determined in accordance with ČSN EN 1015-3. The target range was selected to reproduce the relatively stiff consistency preferred for manual repointing of historic masonry joints.

The freshly cast samples were stored in sealed polyethylene bag. Hardened mortar specimens were demolded after 48 h and subsequently cured under controlled conditions at a temperature (22 ± 2)°C and a relative humidity (65 ± 5)% until testing at 28, 90 and 365 days based on ČSN EN 1015-11.

The substrates comprised Božanov sandstone, Hořice sandstone, brick, and granite, representing common materials used in historic masonry bridges.

These materials exhibit substantial differences in mechanical stiffness and thermal behaviour; consequently, Young's modulus and the coefficient of thermal expansion were considered critical parameters for assessing the likelihood of stress development resulting from incompatibility between the repair mortars and the original masonry.

Young's modulus was determined from the initial linear portion of the force-deflection response recorded during three-point bending. The specimens (20 mm × 20 mm × 100 mm) were supported over a span of 80 mm and loaded at midspan under displacement control at a crosshead rate of 0.15 mm/min. The applied force was measured using a 10 kN load cell (Lukas). The deflection was measured by an LVDT sensor (SOLARTRON) with the maximum stroke up to 1 mm. The slope of the force-deflection curve was determined between 10 % and 40 % of the maximum load. Young's modulus was subsequently calculated using the measured slope, specimen geometry, support span and a shear correction applicable to a rectangular cross-section. Non-standard prismatic specimens were selected to better represent the geometry of repointing mortar joints.

Three replicate specimens were tested for each mortar composition and curing age, and three replicate specimens were also prepared from each masonry substrate for both methods. Measurements were excluded only when the test record indicated an identifiable experimental artefact, such as specimen slippage, loss of sensor contact, or instrument malfunction.

The apparent coefficient of linear thermal expansion (CTE) was determined using a Linseis L76 push-rod dilatometer. Cylindrical specimens approximately 20 mm in length and 10 mm in diameter were tested. The measurements were conducted during heating from 25 to 80 °C at a heating rate of 0.5 °C/min. In addition to the overall temperature range, the subintervals 25–40, 40–60 and 60–80 °C were evaluated to identify temperature-dependent variations that might not be apparent from a single average CTE value. The first heating cycle was excluded from the evaluation, and the reported apparent CTE values were calculated from the second through fourth heating cycles. The measured dilatometric curves were corrected using SRM 739 as the reference material. The apparent coefficient of linear thermal expansion was calculated from the length change between the lower and upper temperature limits.

3. RESULTS

3.1. Young's modulus

The investigated repointing mortars showed considerable variation in Young's modulus depending on binder composition and age (Table 1). M1 showed only a limited increase with age, from 6.15 GPa at 28 days to 6.84 GPa at 365 days. M2 exhibited a progressive increase from 9.49 to 12.62 GPa. The mean Young's modulus of M3 increased between 28 and 90 days and subsequently decreased moderately. M4 showed the largest absolute increase, from 20.01 to 25.53 GPa, whereas M2 exhibited the largest relative increase between 28 and 365 days. M5 remained approximately stable between 28 and 90 days, followed by an increase to 17.93 GPa at 365 days. At 90 and 365 days, M6 exhibited the highest Young's modulus among the investigated mortars, increasing to 32.73 GPa.

The masonry substrates covered a broad stiffness range. Božanov sandstone and brick exhibited the lowest Young's moduli, 2.34 and 2.73 GPa, respectively, whereas Hořice sandstone reached 8.61 GPa and granite 21.70 GPa.

Table 1: *Young's modulus, E (GPa), derived from three-point bending tests for the masonry substrates and repointing mortars at different ages; mean ± standard deviation*

Sample	E (GPa)		
	Substrate/28 d	90 d	365 d
M1	6.15 ± 0.72	6.20 ± 0.43	6.84 ± 0.63
M2	9.49 ± 0.79	10.00 ± 0.27	12.62 ± 0.73
M3	5.38 ± 0.44	6.83 ± 0.35	6.35 ± 0.32
M4	20.01 ± 0.29	21.23 ± 1.48	25.53 ± 0.57
M5	15.17 ± 2.44	14.75 ± 1.04	17.93 ± 1.10
M6	-	25.68 ± 0.54	32.73 ± 3.07
Granite	21.70 ± 1.85	-	-
Brick	2.73 ± 0.45	-	-
Hořice sandstone	8.61 ± 1.64	-	-
Božanov sandstone	2.34 ± 0.20	-	-

3.2. Apparent coefficient of linear thermal expansion

3.2.1. Overall temperature interval of 25–80 °C

The apparent coefficients of linear thermal expansion determined during heating from 25 to 80 °C are presented in Table 2. At 28 days, the mortar values ranged from 8.74 × 10^{-6} K^{-1} for M5 to 10.83 × 10^{-6} K^{-1} for M6. M1–M4 and M6 exhibited similar coefficients at 28 and 90 days, generally between 10 and 11 × 10^{-6} K^{-1}, whereas M5 consistently exhibited lower apparent CTE values than the other mortar formulations.

Changes between 28 and 90 days were relatively limited and mixture-dependent. Among the mortars evaluated at 365 days, the apparent CTE decreased relative to the corresponding 90-day values, reaching 8.52–10.05 × 10^{-6} K^{-1}. The largest decrease between 28 and 365 days was observed for M4, from 10.65 to 9.50 × 10^{-6} K^{-1}, whereas M5 exhibited the smallest change in the mean apparent CTE between 28 and 365 days. Increased variability at 365 days was observed for M1.

The masonry substrates showed two distinct levels of thermal expansion. Granite and brick exhibited nearly identical coefficients of 6.29 and 6.26 × 10^{-6} K^{-1}, respectively. Considerably higher values were measured for Hořice sandstone and Božanov sandstone, reaching 11.47 and 11.98 × 10^{-6} K^{-1}.

The mortar values therefore generally occupied an intermediate range between low CTE and high CTE substrates. At 28 and 90 days, most mortars were closer to the sandstones, with the smallest difference observed between M1 at 90 days and Hořice sandstone.

At 365 days, M5 exhibited the lowest mortar CTE and the smallest difference from granite and brick, although its coefficient remained higher than those of both substrates.

Table 2: *Apparent coefficients of linear thermal expansion during heating, α_{25-80} (×10^{-6} K^{-1}), of the masonry substrates and repointing mortars at different ages; mean ± standard deviation*

Sample	α(×10^{-6} K^{-1})		
	Substrate/28 d	90 d	365 d
Granite	6.29 ± 0.20	-	-
Brick	6.26 ± 0.20	-	-
Hořice sandstone	11.47 ± 0.86	-	-
Božanov sandstone	11.98 ± 0.14	-	-
M1	10.18 ± 0.20	10.97 ± 0.13	9.55 ± 1.00
M2	10.25 ± 0.18	10.45 ± 0.25	9.89 ± 0.68
M3	10.17 ± 0.21	10.09 ± 0.29	9.90 ± 0.22
M4	10.65 ± 0.25	10.33 ± 0.21	9.50 ± 0.45
M5	8.74 ± 0.69	9.50 ± 0.42	8.52 ± 0.53
M6	10.83 ± 0.17	10.51 ± 0.38	10.05 ± 0.31

3.2.2. Subintervals 25–40, 40–60 and 60–80 °C

The subinterval analysis revealed temperature-dependent differences in thermal expansion behaviour (Tables 3 and 4). M1 showed increasing apparent CTE values across the three subintervals, most clearly at 28 and 90 days. M2 and M4 at 28 and 90 days, together with M6 at 28 days, exhibited higher values in the 40–60 °C interval than in the adjacent intervals. For M5 at 28 days, the mean apparent CTE decreased across the three subintervals.

Table 3: *Apparent coefficients of linear thermal expansion, α (×10^{-6} K^{-1}), determined during heating in different temperature subintervals for the repointing mortars at different ages; mean ± standard deviation*

Mortar	Age (days)	α (×10^{-6} K^{-1})		
		25–40	40–60	60–80
M1	28	8.58 ± 0.09	10.58 ± 0.30	10.98 ± 0.29
	90	9.69 ± 0.06	11.40 ± 0.16	11.49 ± 0.25
	365	8.31 ± 1.27	9.74 ± 1.09	10.27 ± 0.71
M2	28	9.85 ± 0.18	10.77 ± 0.17	10.03 ± 0.25
	90	9.86 ± 0.39	11.17 ± 0.24	10.17 ± 0.36
	365	8.84 ± 1.41	10.55 ± 0.50	10.02 ± 0.35
M3	28	9.75 ± 0.13	10.52 ± 0.21	10.14 ± 0.27
	90	9.20 ± 0.46	10.53 ± 0.31	10.32 ± 0.18
	365	9.21 ± 0.21	10.22 ± 0.25	10.11 ± 0.23
M4	28	9.95 ± 0.34	11.40 ± 0.26	10.43 ± 0.31
	90	9.62 ± 0.51	11.10 ± 0.19	10.08 ± 0.25
	365	8.65 ± 0.95	10.12 ± 0.41	9.52 ± 0.25
M5	28	9.02 ± 0.35	9.01 ± 0.70	8.27 ± 0.38
	90	9.41 ± 0.98	10.13 ± 0.44	8.94 ± 0.46
	365	7.95 ± 0.62	9.14 ± 0.57	8.34 ± 0.56
M6	28	10.44 ± 0.33	11.70 ± 0.08	10.27 ± 0.27
	90	9.38 ± 0.84	11.14 ± 0.47	10.71 ± 0.20
	365	9.40 ± 0.61	10.73 ± 0.31	9.82 ± 0.26

Table 4: *Apparent coefficients of linear thermal expansion, α (×10^{-6} K^{-1}), determined during heating in different temperature subintervals for the masonry substrates; mean ± standard deviation*

Substrate	α (×10^{-6} K^{-1})		
	25–40	40–60	60–80
Granite	4.72 ± 0.44	6.59 ± 0.24	7.18 ± 0.03
Brick	5.63 ± 0.22	6.51 ± 0.23	6.49 ± 0.17
Hořice sandstone	9.07 ± 0.90	11.99 ± 0.90	12.75 ± 0.79
Božanov sandstone	10.24 ± 0.17	12.42 ± 0.17	12.83 ± 0.07

Both sandstones exhibited increasing apparent CTE values with temperature. In the 40–60 and 60–80 °C intervals, their coefficients were higher than those of all investigated mortars. At 25–40 °C, however, the mortar and sandstone values partly overlapped. Granite also showed an increase across the investigated temperature range, whereas the apparent CTE of brick remained nearly constant above 40 °C. In all subintervals, granite and brick exhibited lower apparent CTE values than all investigated mortars.

4. DISCUSSION

The results demonstrate that apparent CTE and Young's modulus provide different but complementary information on mortar-substrate behaviour. Close correspondence in thermal expansion did not necessarily coincide with close correspondence in stiffness, indicating that neither parameter alone is sufficient for assessing potential thermo-mechanical mismatch. The difference in CTE between the mortar and substrate determines their differential free thermal strain during a temperature change, whereas the stresses that may develop under restraint are also influenced by the stiffness of the interacting materials [3].

The two properties differed in the magnitude and pattern of their age-related changes. Young's modulus varied markedly among the mortar formulations, with pronounced increases observed for several mixtures, particularly blended mortars M2 and M4 as well as the white cement M6. In contrast, the overall apparent CTE values remained within a comparatively narrow range. At 365 days, the mean apparent CTE was lower than

the corresponding 90-day value for all investigated mortars, although the magnitude of the decrease varied among the mortar formulations. These results indicate that the mechanical and thermal properties may develop differently with age. The development may be attributed to continued hydration, carbonation, and associated microstructural changes [4, 5].

The subinterval analysis further showed that the mortar-substrate CTE relationship depended on temperature. At 25–40 °C, the mean apparent CTE values of both sandstones fell within the range observed for the mortars. In the 40–60 and 60–80 °C intervals, however, both sandstones exhibited higher mean apparent CTE values than all investigated mortars, and the CTE difference between the mortars and sandstones therefore became more pronounced at higher temperatures. Granite and brick showed a different relationship, with apparent CTE values below those of all mortars throughout the investigated temperature range. The overall α25–80 value does not fully capture the temperature-dependent variation in the mortar-substrate relationship.

The combined comparison of CTE and stiffness showed that the relative suitability of the mortars depended on the substrate considered. For Hořice sandstone, M1 (NHL) showed the smallest overall CTE difference, particularly at 90 days, whereas M2 showed the closest correspondence in Young's modulus at 28 and 90 days. Božanov sandstone presented a different situation because of its considerably lower stiffness. M1 and M3 (NHL–Roman cement) had the lowest Young's moduli among the investigated mortars, but both remained substantially stiffer than this substrate. For granite, M5 (Roman cement) showed the smallest overall CTE difference while remaining less stiff than the substrate throughout the investigated period. M4 showed the closest stiffness correspondence at 28 and 90 days but exceeded the Young's modulus of granite at 365 days. For brick, none of the investigated mortars approached both its low CTE and low stiffness: M1 and M3 showed the smallest stiffness differences, whereas M5 showed the smallest CTE difference. M6 (white Portland cement) was stiffer than all investigated substrates at the ages evaluated, resulting in the greatest stiffness contrast.

The present assessment provides a qualitative indication of potential thermo-mechanical mismatch rather than a direct prediction of stresses in a repointed joint. Since no quantitative compatibility threshold was applied, similarities in CTE or stiffness should be interpreted as comparative indicators rather than direct evidence of in-situ compatibility.

5. CONCLUSION

The investigated repointing mortars exhibited substantially greater differences in stiffness whereas their overall apparent coefficients of linear thermal expansion varied within a comparatively narrow range, with both properties exhibiting age-dependent changes. The overall α25–80 values of all mortars lay between those of the low-CTE granite and brick and the higher-CTE sandstones, while the subinterval analysis showed that the CTE mismatch between the mortars and sandstones became more pronounced at higher temperatures.

The combined evaluation of CTE and Young's modulus revealed different relationships for the individual substrates. For Hořice sandstone, M1 (NHL) showed close CTE correspondence together with comparatively low stiffness, while M2 (NHL-Roman cement) showed the closest stiffness correspondence at 28 and 90 days. For the low-modulus Božanov sandstone, M1 and M3 (NHL-Roman cement) showed the smallest stiffness differences among the investigated mortars, although a substantial mismatch remained. M5 (Roman cement) showed the smallest CTE difference from granite while remaining less stiff than the substrate. For brick, no mortar simultaneously approached both its low CTE and low stiffness.

These results demonstrate that assessment based on CTE and stiffness does not necessarily lead to the same ranking of mortar-substrate combinations and that mortar selection should therefore be substrate-specific. The results provide a basis for a qualitative assessment of potential thermo-mechanical mismatch in repointed masonry; direct quantification of the resulting stresses would require additional analysis.

5. REFERENCES

[1] TC 203-RHM (Main author: Hughes, J.J.). RILEM TC 203-RHM: Repair mortars for historic masonry. The role of mortar in masonry: An introduction to requirements for the design of repair mortars. Mater. Struct. 2012, 45, 1287–1294.

[2] TC 203-RHM (Main author: Lindqvist, J.E.). RILEM TC 203-RHM: Repair mortars for historic masonry. Testing of hardened mortars, a process of questioning and interpreting. Mater. Struct. 2009, 42, 853–865.

[3] Drdácký, M.; Beran, P. Compatible dilation limits of masonry joint mortars. Int. J. Archit. Herit. 2010, 4, 155–176.

[4] Groot, C.; Veiga, R.; Papayianni, I.; Van Hees, R.; Secco, M.; Alvarez, J.I.; Faria, P.; Stefanidou, M. RILEM TC 277-LHS report: Lime-based mortars for restoration–a review on long-term durability aspects and experience from practice. Mater. Struct. 2022, 55, 245.

[5] Röttger, A.; Youn-Čale, B.-Y.; Küpferle, J.; Lentz, J.; Breitenbücher, R.; Theisen, W. Time-dependent evolution of microstructure and mechanical properties of mortar. Int. J. Civ. Eng. 2019, 17, 61–74.

Authors:

Ing. Pavla Náhunková – The Institute of Theoretical and Applied Mechanics, Czech Academy of Sciences, Department of Materials Research, Prosecká 809/76, 19000, Prague 9, Czech Republic. e-mail: nahunkova@itam.cas.cz

Mgr. Dita Frankeová, Ph.D. – The Institute of Theoretical and Applied Mechanics, Czech Academy of Sciences, Department of Materials Research, Prosecká 809/76, 19000, Prague 9, Czech Republic.

Mgr. Petra Mácová – The Institute of Theoretical and Applied Mechanics, Czech Academy of Sciences, Department of Materials Research, Prosecká 809/76, 19000, Prague 9, Czech Republic.

Ing. Jiří Kunecký, Ph.D. – The Institute of Theoretical and Applied Mechanics, Czech Academy of Sciences, Department of Applied Mechanics and Structures, Prosecká 809/76, 19000, Prague 9, Czech Republic.

ACKNOWLEDGEMENTS

The research was carried out with the support of the Czech Ministry of Culture, project NAKI III DH23P03OVV024. The text was refined by ChatGPT.

MECHANICAL AND CHROMATIC RESPONSE OF COARSE-GRAINED SANDSTONE SUBJECTED TO ELEVATED TEMPERATURES

ZMĚNY MECHANICKÝCH VLASTNOSTÍ A BARVY HRUBOZRNNÉHO PÍSKOVCE VLIVEM VYSOKÝCH TEPLOT

Ema Jankovičová[1] and Radek Zigler[2,]*

Abstract
Natural stone has been widely used in masonry structures, including churches and cathedrals, due to its availability and favourable mechanical properties. Many of these structures have been preserved and constitute an important component of cultural heritage. Although stone is generally considered a non-combustible material, exposure to high temperatures can substantially alter its physical and mechanical behaviour. This study investigates the effects of elevated temperatures on the mechanical properties of coarse-grained sandstone. Specimens were subjected to thermal loading in an electric furnace at temperatures up to 1100 °C, followed by two different cooling regimes: slow cooling within the furnace and rapid quenching in water. In addition to mechanical testing, colour changes induced by thermal exposure were also assessed. The results demonstrated a decline in compressive strength and modulus of elasticity, an increase in axial deformation, and a pronounced change in colour, all dependent on the level of thermal loading.

Abstract
Přírodní kámen se pro svou dostupnost a příznivé mechanické vlastnosti široce využíval ve zděných konstrukcích, včetně kostelů a katedrál. Řada těchto staveb se dochovala a tvoří významnou součást kulturního dědictví. Přestože je kámen obecně považován za nehořlavý materiál, vystavení vysokým teplotám může podstatně změnit jeho fyzikální a mechanické chování. Článek se věnuje vlivu vysokých teplot na mechanické vlastnosti hrubozrnného pískovce. Vzorky byly podrobeny tepelnému zatížení v elektrické peci při teplotách až 1100 °C a následně ochlazovány dvěma různými způsoby: pomalým chladnutím v peci a rychlým ochlazením ve vodě. Kromě mechanických zkoušek byly vyhodnoceny také barevné změny vyvolané tepelným působením. Výsledky prokázaly pokles pevnosti v tlaku a modulu pružnosti, nárůst osové deformace a výraznou změnu barvy v závisloti na úrovni teplotního zatížení.

Key words: *Božanov sandstone; thermal degradation; water quenching; mechanical properties; colour alteration*

1. INTRODUCTION

Fire exposure poses a significant risk to historic masonry, as elevated temperatures can adversely affect both the structural integrity and the conservation of historically valuable materials. In contrast to modern construction, historic buildings frequently contain original masonry components for which the initial material properties and previous thermal history may be difficult to determine following a fire. A reliable evaluation of fire-affected stone is therefore essential when determining whether damaged elements can remain in situ, be repaired, or need to be replaced.

The response of natural stone to high temperatures involves a range of physical and microstructural processes, including thermal expansion, moisture evaporation, mineralogical changes, and microcrack development. These processes can result in a loss of mechanical strength and stiffness and modify the deformation characteristics of the material [1, 2]. The cooling stage following thermal exposure can further influence the resulting damage, particularly when water quenching is applied during firefighting [3]. Rapid cooling may generate additional thermal stresses and consequently intensify the deterioration. Thermal exposure is also commonly accompanied by visible colour changes, which can provide a practical indication of fire-induced alteration [4, 5].

Sandstone represents an important component of historic masonry in the Czech Republic. Previous research has demonstrated that the thermal response of sandstone is strongly dependent on its mineralogical and microstructural characteristics. This study examines the effects of exposure to 690, 850, and 1100 °C, followed by either furnace (oven) cooling (OC) or water quenching (WC), on the compressive strength, axial strain, Young's modulus, and CIELAB colour parameters of Božanov sandstone. The main findings of previous studies

concerning thermal degradation and colour alteration are summarised in the following section.

State of the Art

The thermal response of natural stone is governed by its mineralogical composition, cementing material, heating regime, and cooling conditions. Previous studies have investigated changes in mechanical properties, porosity, density, wave velocity, microstructure and colour following thermal exposure. Leroy et al. [6] identified approximately 400 °C as an important temperature for sandstone and granite, above which substantial mechanical degradation may occur. The α-β quartz transition at 573 °C causes volumetric expansion and microcracking in quartz-rich rocks, while porosity increases rapidly above approximately 500 °C.

For sandstone, Keppert et al. [7] demonstrated that thermal behaviour is strongly controlled by mineralogical composition and cementing material. Siliceous sandstones experienced significant strength reduction due to thermal cracking, whereas clayey sandstones showed increased compressive strength related to dehydroxylation and sintering of clay minerals.

Moghrabi et al. [8], identified approximately 400 °C as an important transition, above which thermal cracking intensified, and compressive strength and P-wave velocity decreased markedly. The study also reported increasingly redder colours with temperature, attributed to iron oxidation.

The influence of fire conditions was demonstrated by Wasantha et al. [9] compared with controlled linear heating, exposure to a modified hydrocarbon fire caused substantially greater degradation, with reductions in compressive strength, elastic modulus and tensile strength of 79.2 %, 90 % and 84.7 %, respectively. Extensive inter- and intra-granular cracking was observed after the intense fire exposure. These results demonstrate that the heating regime can significantly influence the residual mechanical properties of sandstone.

Studies on other natural stones further indicate that mechanical deterioration is not necessarily immediate at moderate temperatures. Mosaddegh et al. [10], reported an initial increase in compressive strength after heating to 100 °C, while repeated thermal cycles caused strength reduction and increased fatigue for marble and travertine. For limestone, Gomah et al. [2], similarly observed an increase in compressive strength up to 400 °C followed by a sharp decrease at higher temperatures, together with increasing porosity and crack density.

Cooling conditions can also influence residual properties. Lobarinhas et al. [3], reported reduced compressive strength and increased water absorption after heating and rapid water cooling, while Lobarinhas et al. [11], demonstrated that thermal damage could already be detected at 300 °C and became more pronounced at 600 °C.

Thermal exposure also produces visible changes in stone colour. Hatır et al. [4], reported a transition from yellowish tones to dark brown between 400 and 500 °C, followed by light brick-red colours above 500 °C, associated with the transformation of magnetite into hematite. Similarly, Fransozo et al. [5], observed pronounced reddish coloration and reduced gloss after fire exposure, attributed to iron oxidation and dehydroxylation of phyllosilicates. These changes were accompanied by intergranular porosity, cracking and reduced compressive strength.

Overall, the reviewed studies indicate that approximately 400 - 500 °C represents an important transition range in the thermal response of sandstone, with accelerated cracking and mechanical degradation generally becoming more pronounced above this range. However, this should not be considered a universal critical temperature, as the response depends on mineralogical composition, heating regime and cooling conditions. While mechanical deterioration has been extensively studied, the relationship between quantitative colour change and residual mechanical properties of sandstone after fire exposure remains less explored, providing a basis for further investigation.

2. MATERIALS AND METHODS

The study focuses on Božanov sandstone, a coarse-grained sandstone with a clastic framework composed predominantly of detrital quartz and quartz-rich quartzite fragments. Quartz is mainly of magmatogenic origin, with fine fluid inclusions. Feldspars are represented by orthoclase, microcline, and plagioclase (oligoclase–andesine) and are variably fractured and argillitized. The rock also contains strongly altered fragments, primarily of originally glassy acidic volcanic rocks. The groundmass is clayey–quartzose, occupying the pores between the clastic grains. Clay minerals are dominated by illite, while quartz also contributes to the cement. Thin illitic clay rims occur around some grains, and some quartz and quartzite grains show thin rims of authigenic quartz [12].

A total of 18 cylindrical specimens, with a nominal diameter of approximately 35 mm and a height of 70 mm, were used for the experimental programme (Figure 1). Thermal treatment was carried out in an electric muffle furnace. The selected temperatures of 690, 850, and 1100 °C were defined based on the results of previous experiments, together with findings reported in the relevant literature. Three specimens were maintained in the untreated state and used as reference samples. The remaining specimens were exposed to temperatures of 690 °C (n = 3), 850 °C (n = 6), and 1100 °C (n = 6).



Figure 1: *Sandstone samples*

Thermal treatment comprised controlled heating at 16 - 18 °C min^{-1}, followed by a dwell of approximately 1 h at the target temperature (± 50 °C). Specimens heated to 850 °C and 1100 °C were subsequently either furnace-cooled (n = 3 per temperature) or water-quenched for approximately 2 min (n = 3 per temperature). The 690 °C specimens were furnace-cooled. Reference specimens remained untreated (Figure 2).

Uniaxial compression tests were conducted using a LabTest 4.100.SP1 testing machine with a maximum load capacity of 100 kN under displacement control at 0.25 mm min^{-1}. Surface deformation was monitored using Digital Image Correlation (DIC) with a LaborTech AOX--ONE camera equipped with a 5 Mpx Blackfly BFS-U3-51S5M sensor (2448 × 2048 px) and a 50 mm lens. The system complied with EN ISO 9513 accuracy class 0.5 and ASTM E83 Class A and was calibrated using a Fiducial Grid with a 5 mm point spacing. A stochastic dot pattern was applied to the specimen surfaces prior to testing.

Thermally induced colour changes were evaluated from photographs acquired before and after thermal treatment. A Canon EOS 60D camera was used to acquire the images under controlled illumination, provided by two diffused reflectors (5000 K) against a neutral infinite background. For each specimen, the mean L*, a*, and b* coordinates were determined independently from ten Regions of Interest (ROIs) selected in the images acquired before and after thermal treatment. The resulting mean CIELab coordinates were compared on a specimen-by-specimen basis, and the total colour difference ΔE was calculated to quantify the thermally induced colour change.

3. RESULTS AND DISCUSSION

The reference specimens showed an average compressive strength of 54.75 MPa (100 %), ranging from 44.98 to 60.56 MPa (82 % - 111 %). After heating to 690 °C, the average strength decreased to 32.62 MPa (60 %) (29.02 MPa - 37.19 MPa; 53 - 68%). At 850 °C, the average strength was 30.92 MPa (56 %) after furnace cooling (27.19 MPa - 33.62 MPa; 50 % - 61 %) and 19.09 MPa

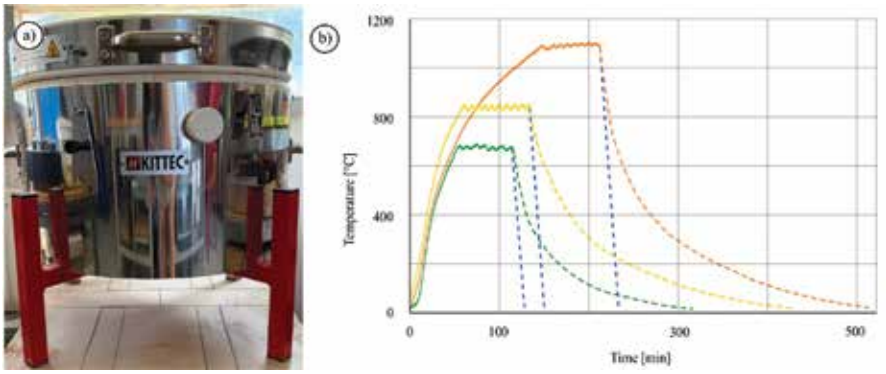


Figure 2: *a) Electric muffle furnace, b) Heating-cooling curves for Sandstone samples.*

(35 %) after water quenching (18.78 MPa - 19.38 MPa; 34 % - 35 %). At 1100 °C, the corresponding values were 17.81 MPa (33 %) for furnace cooling (16.26 MPa - 19.77 MPa; 30 % - 36 %) and 8.41 MPa (15 %) for water quenching (5.65 MPa - 11.21 MPa; 10 % - 20 %). Overall, compressive strength decreased with increasing temperature, with water quenching resulting in a further reduction.

The reference specimens exhibited an average axial strain of 0.00201 (100 %), with values ranging from 0.00166 to 0.00226 (83 % - 113%). After heating to 690 °C, the average strain increased to 0.00405 (202 %) (0.00387 - 0.00426; 193 % - 212 %). At 850 °C, the average strain reached 0.00536 (267 %) after furnace cooling (0.00470 - 0.00594; 234 % - 296 %) and 0.01274 (635 %) after water quenching (0.01219 - 0.01322; 608 % - 659 %). At 1100 °C, the corresponding values were 0.01111 (554 %) for furnace cooling (0.01089 - 0.01147; 543 % - 572 %) and 0.01114 (555 %) for water quenching (0.01012 - 0.01187; 504 % - 592 %). Overall, axial strain increased substantially with thermal exposure, with the most pronounced increase observed after water quenching at 850 °C.

The reference specimens showed an average Young's modulus of 36.802 GPa (100 %), ranging from 26.387 to 47.031 GPa (72 % - 128 %). After heating to 690 °C, the average decreased to 15.941 GPa (43 %) (14.853 GPa - 17.562 GPa; 40 % - 48 %). At 850 °C, the average modulus was 11.411 GPa (31 %) after furnace cooling (10.879 GPa - 11.821 GPa; 30 % - 32 %) and 3.715 GPa (10 %) after water quenching (3.648 GPa - 3.769 GPa; ~10 %). At 1100 °C, the corresponding values were 3.153 GPa (9 %) for furnace cooling (2.794 GPa - 3.735 GPa; 8 % - 10 %) and 1.420 GPa (4 %) for water quenching (0.878 GPa - 1.886 GPa; 2 % - 5 %). Overall, Young's modulus decreased markedly with increasing temperature, with water quenching producing the lowest values.

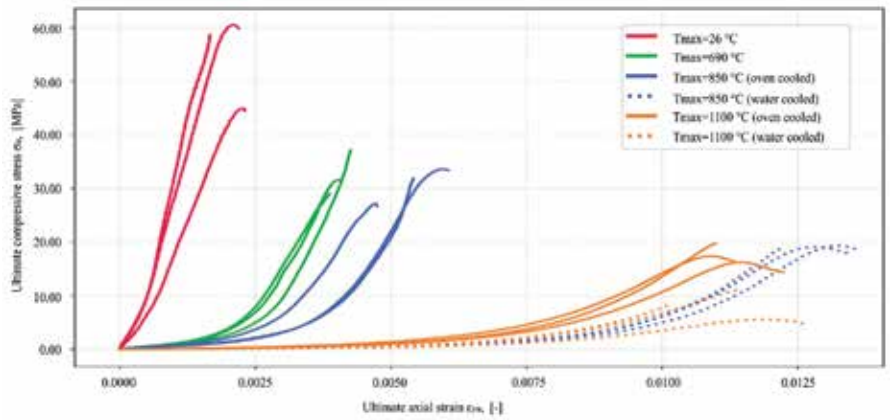


Figure 3: *Stress–strain relationship of Sandstone samples under uniaxial compression.*

The effects of heating and cooling are also reflected in the stress–strain curves (Figure 3). The reference specimens exhibited the highest strength and steepest slope, with an almost linear increase in stress. With increasing temperature, the slope gradually decreased and the initially linear response became increasingly nonlinear, approaching an exponential behaviour. A substantially different response was observed for specimens heated to 850 °C and water quenched, as well as for specimens heated to 1100 °C under both cooling conditions. These specimens exhibited pronounced deformation already during the initial loading stage. After this initial deformation, a slight increase in load was observed until the maximum load-bearing capacity was reached, followed by specimen collapse. The most pronounced deformation was recorded for the 850 °C water-cooled specimens. Although the 1100 °C specimens exhibited similar pronounced initial deformation, following the same overall trend, their more severe thermal degradation resulted in an earlier loss of load-bearing capacity and collapse. In contrast, the 850 °C specimens were able to sustain higher loads and therefore undergo greater deformation before failure.

One-way ANOVA confirmed a significant effect of temperature on compressive strength, axial strain, and Young's modulus for both furnace-cooled specimens ($F(3,8) = 27.03$, 296.9, and 22.59, respectively; $p < 0.001$) and water-cooled specimens ($F(2,6) = 66.04$, 252.3, and 33.03, respectively; $p < 0.001$). Post hoc analysis confirmed significant differences between the reference and thermally treated groups for all three mechanical parameters ($p \leq 0.005$).

Two-way ANOVA further demonstrated significant effects of both cooling regime and temperature on axial strain, compressive strength, and Young's modulus ($p < 0.001$). A significant temperature and cooling interaction was observed for axial strain ($F(1,8) = 102.31$, $p < 0.001$) and Young's modulus ($F(1,8) = 141.6$, $p < 0.001$), whereas the interaction was not significant for compressive strength ($F(1,8) = 0.795$, $p = 0.399$).

Thermal exposure resulted in distinct changes in the CIELAB colour parameters (Figure 4), accompanied by visible colour alterations of the sandstone specimens (Figure 5). The L* value decreased slightly from 41.944 for the reference specimens to 39.038 at 690 °C, followed by an increase to 53.170 and 52.691 after heating to 850 °C with furnace and water cooling, respectively. At 1100 °C, L* remained similar after furnace cooling (53.397) and increased further after water cooling (55.074). The a* coordinate increased from 5.509 to 7.328 at 690 °C and reached 10.641 (furnace cooling) and 12.533 (water cooling) at 850 °C. At 1100 °C, it decreased to 8.927 and 8.275, respectively. The b* coordinate showed only a minor change at 690 °C, from 13.619 to 12.267, increased to 18.585 and 21.589 at 850 °C, and subsequently decreased to 16.452 and 15.055 at 1100 °C. The total colour difference ΔE increased from 6.275 at 690 °C to 12.136 and 12.028 at 850 °C for furnace- and water-cooled specimens, respectively. At 1100 °C, ΔE remained comparable at 12.279 after furnace cooling and increased slightly to 13.079 after water cooling.

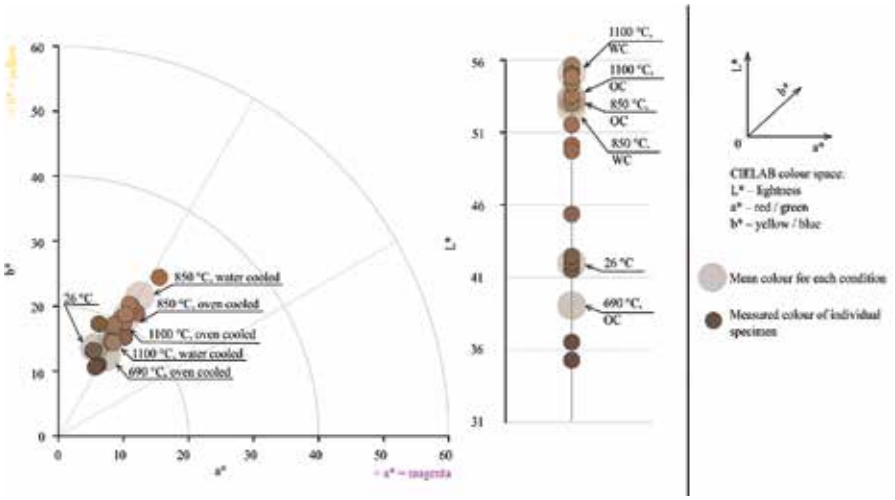


Figure 4: *CIELab colour parameters of Sandstone specimens subjected to elevated temperatures; OC – oven-cooled, WC - water-cooled.*

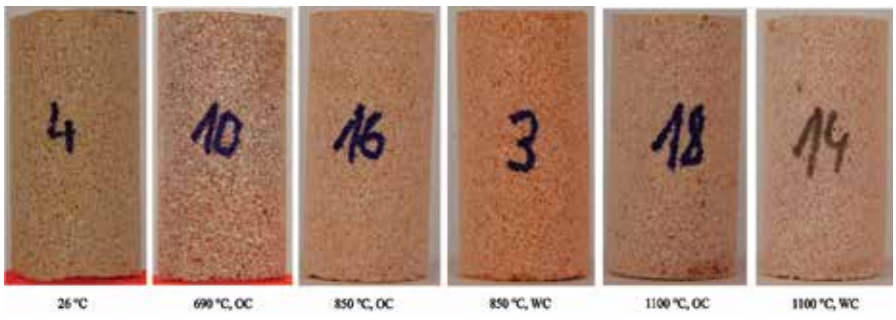


Figure 5: *Visual appearance of Božanov sandstone specimens after thermal exposure at different temperatures and cooling conditions; OC – oven-cooled, WC - water-cooled.*

Although both colour parameters and mechanical properties changed significantly with increasing temperature, no direct correlation between colour change and mechanical degradation was observed. In particular, ΔE increased markedly up to 850 °C but remained relatively stable at higher temperatures, whereas compressive strength and Young's modulus continued to decrease substantially. Therefore, based on the current findings, colour change can be considered an indicator of thermal alteration of the sandstone, but it does not provide a reliable quantitative measure of the resulting mechanical degradation.

5. CONCLUSION

The results clearly demonstrate the influence of both heating temperature and cooling regime on the mechanical properties of Božanov sandstone. Increasing temperature resulted in a progressive decrease in compressive strength and Young's modulus, accompanied by an increase in axial strain. The effect of thermal exposure was also evident in the stress - strain response, which progressively changed from an almost linear behaviour in the reference specimens to nonlinear and ultimately exponential behaviour at higher temperatures. After

exposure to 1100 °C, pronounced deformation occurred already during the initial loading stage.

Thermal exposure also produced significant colour changes, with the most pronounced alteration observed after heating to 850 °C. At higher temperature, however, the colour parameters changed only slightly, in contrast to the continued and substantial deterioration of the mechanical properties. This indicates that although colour alteration clearly reflects thermal exposure, it does not directly correspond to the extent of mechanical degradation.

6. REFERENCES

[1] R. Zigler, E. Jankovičová, K. Kovářová, E. Matoušková, P. Ryparová, and T. Čejka, 'Experimental Assessment of Post-Fire Residual Material Properties of Marlstone', *Heritage*, vol. 9, no. 2, p. 76, Feb. 2026, doi: 10.3390/heritage9020076.

[2] M. E. Gomah, E. Wang, A. A. Omar, Z. Du, and M. M. Zaki, 'Mineralogical and microstructural study of thermally treated Egyptian limestone and the related modifications to its physico-mechanical properties', *J Therm Anal Calorim*, vol. 151, no. 3, pp. 2715–2737, Feb. 2026, doi: 10.1007/s10973-025-15242-0.

[3] R. Lobarinhas, G. Paneiro, and A. Dionísio, 'A penalty-based evaluation framework for assessing the post-fire functional suitability of carbonate architectural stones', *Mater Struct*, vol. 59, no. 1, p. 11, Dec. 2025, doi: 10.1617/s11527-025-02898-1.

[4] M. E. Hatır, İ. İnce, M. Korkanç, and M. Ş. Ataş, 'Spectrophotometer-Based Novel Models for Detection of Fire Damage in Stone Monuments', *Geoheritage*, vol. 18, no. 2, p. 91, Apr. 2026, doi: 10.1007/s12371-026-01322-6.

[5] H. L. Fransozo, G. F. C. Lima, A. M. C. de Gouveia, and A. C. da Silva Bezerra, 'Fire effects on itacolomi quartzites from stonework historical buildings: implications for conservation of the cultural heritage', *J Build Rehabil*, vol. 9, no. 2, p. 135, Aug. 2024, doi: 10.1007/s41024-024-00490-8.

[6] M. N. Luc Leroy, F. W. Marius, and N. François, 'Experimental and Theoretical Investigations of Hard Rocks at High Temperature: Applications in Civil Engineering', *Advances in Civil Engineering*, vol. 2021, no. 1, p. 8893944, 2021, doi: 10.1155/2021/8893944.

[7] M. Keppert *et al.*, 'Behavior of Sandstones Under Heat Treatment', *Int J Thermophys*, vol. 38, no. 4, p. 60, Feb. 2017, doi: 10.1007/s10765-017-2191-0.

[8] R. Moghrabi, Á. Török, and B. Vásárhelyi, 'High Temperature Effects on the Engineering Properties of Sandstone', *Rock Mechanics Letters*, vol. 3, no. 1, pp. 295–301, Jan. 2026, doi: 10.70425/rml.202601.37.

[9] P. L. P. Wasantha, K. Cranfield-Brooks, W. G. P. Kumari, T. Xu, and M. Guerrieri, 'Fire-induced mechanical transformations in Hawkesbury sandstone: Experimental observations and analysis', *International Journal of Rock Mechanics and Mining Sciences*, vol. 190, p. 106110, Jun. 2025, doi: 10.1016/j.ijrmms.2025.106110.

[10] A. Mosaddegh, A. Fahimifar, and P. Najafipour, 'Influence of thermal and cooling cycles on the mechanical properties of building stones with carbonate texture', *Geothermics*, vol. 130, p. 103330, Jul. 2025, doi: 10.1016/j.geothermics.2025.103330.

[11] R. Lobarinhas, G. Paneiro, and A. Dionísio, 'Diagnosis of thermal degradation in carbonate building stones using the felicity ratio', *Journal of Building Engineering*, vol. 119, p. 115299, Feb. 2026, doi: 10.1016/j.jobe.2026.115299.

[12] 'Dekorační kameny, vápence a vybrané písky ČR - Božanov'. Accessed: Aug. 28, 2026. [Online]. Available: http://kamenolomy.fzp.ujep.cz/index.php?page=record&id=127&tab=petro

Authors:

Ing. Ema Jankovičová – Czech Technical university in Prague, Faculty of Civil Engineering, Department or Architectural Engineering, Thákurova 2077/7, 166 29 Prague, Czech Republic, e-mail: jankoema@cvut.cz

Ing. Radek Zigler, Ph.D. – Czech Technical university in Prague, Faculty of Civil Engineering, Department or Architectural Engineering, Thákurova 2077/7, 166 29 Prague, Czech Republic, e-mail: zigler@fsv.cvut.cz

ACKNOWLEDGEMENTS

This research was funded by internal CTU grant SGS26/147/OHK1/3T/11 „Analysis of the Dependence of the Physico-Mechanical Properties of Selected Building Materials on Thermal Loading ".

CATHODIC PROTECTION AS AN INNOVATIVE REHABILITATION TECHNIQUE WITH CASE STUDIES FROM GERMANY

KATODICKÁ OCHRANA JAKO INOVATIVNÍ SANAČNÍ METODA S PŘÍPADOVÝMI STUDIEMI Z NĚMECKA

Hernâni Esteves, CATÓDICA GmbH, Mönchengladbach, Germany
Andreas Tobler, CATÓDICA GmbH, Mönchengladbach, Germany

Abstract
Cathodic protection offers a practical way to control reinforcement corrosion and retain serviceable concrete during the rehabilitation of existing structures. Its application is illustrated by three underground car parks in Germany: the AfA car park in Paderborn, the NRW Bank car park in Münster and the car park at Scharnhorststraße 44–48 in Münster. The projects cover the full sequence from damage assessment and in situ investigations through design and installation to commissioning. In Paderborn, discrete anodes protect column bases, foundations, beams and slab soffits. At the two Münster sites, titanium ribbon anodes provide protection over extensive floor areas and at the bases of walls and columns. The installations comprise 6, 20 and 43 independently controlled protection zones. Together, the projects show how anode systems, installation details and monitoring can be adapted to the geometry and condition of existing concrete structures. Compared with conventional concrete replacement, CP can reduce concrete removal, temporary propping and closure periods, limiting disruption and potential revenue losses. Retaining sound concrete can also reduce waste, demand for replacement materials and the carbon footprint of rehabilitation.

Keywords: *cathodic protection; reinforced concrete; chloride induced corrosion; underground car parks; rehabilitation; commissioning.*

1 INTRODUCTION

Underground car parks are regularly exposed to water and de icing salts carried in by vehicles. Chlorides can penetrate the concrete through cracks and unprotected surfaces, particularly at floor level and around wall and column bases. Once the passive protection of the reinforcement is disturbed, corrosion can develop within concrete that may still appear sound. Rehabilitation therefore needs to address both the visible damage and the conditions affecting the embedded steel.

Cathodic protection (CP) controls this corrosion by supplying a protective current to the reinforcement. It can be combined with local concrete repairs, allowing suitable existing concrete to remain in place [1, 5]. The following three projects illustrate how the technique is planned and installed in practice, from the initial investigations to the first performance checks.

2 PRINCIPLES OF CATHODIC PROTECTION

2.1 Electrochemical action

In reinforced concrete, corrosion develops through anodic dissolution of steel and cathodic reactions elsewhere on the reinforcement. Chlorides can disrupt the passive condition normally provided by the alkaline concrete. An impressed current CP system supplies current through an auxiliary anode embedded in, or applied to, the concrete. The anode is connected to the positive terminal of a direct current supply, while the reinforcement is connected to the negative terminal. Current flows through the concrete pore solution towards the steel, shifting its potential in the negative direction and reducing anodic dissolution [1].

The anode and reinforcement are electrically separated, with a compatible cementitious material providing the ionic connection between them. The reinforcement within each cathode circuit must be electrically continuous, or its separate sections must be accommodated in the design. Concrete cover, reinforcement layout and member geometry determine where anodes can be installed and how the protective current reaches the steel. Particular care is needed during installation to prevent direct contact between the anodes and reinforcement [1].

2.2 Investigation and design

The initial investigations establish the condition of the concrete and reinforcement and define the areas to be protected. Visual inspections are combined with cover measurements, continuity testing, potential mapping and concrete testing. Chloride profiles establish the depth and extent of contamination. Concrete resistivity measurements help assess current distribution and identify the influence of moisture or previous repair materials. Potential maps indicate areas with a higher likelihood of corrosion and guide the selection of locations for closer inspection and monitoring [1].

The required protective current is cal-

culated from the steel surface area and the design current density. The anode type and spacing are selected to supply this current across the intended protection area. Dividing the installation into independently controlled zones allows the current supply to be adapted to different members and exposure conditions. Embedded reference electrodes measure the response of the reinforcement, while the control system records current, voltage and potential. Concrete repair, crack treatment and any necessary structural strengthening are carried out as part of the overall rehabilitation [1].

2.3 Commissioning and protection assessment

Before energisation, the connections, polarity, continuity, insulation and measurement channels are checked. The zones are then brought into operation in stages, with measurements taken at short intervals so that the response can be observed closely. The steel potential shifts in the negative direction as the protective current is applied. Subsequent performance checks establish whether the required protection criteria have been reached [1].

One of the protection criteria in ISO 12696:2022 is a depolarisation of at least 100 mV within a maximum of 24 hours, measured from the instant off potential after interrupting the protective current. The immediate ohmic voltage change is excluded from this assessment. Alternative criteria and negative potential limits are also available. Absolute potentials are evaluated against the specified reference electrode and electrolyte. Where prestressed or high strength steel is present, the permissible potential range requires a specific assessment [1].

3 AFA UNDERGROUND CAR PARK IN PADERBORN

3.1 Project description and condition

The AfA facility at Bahnhofstraße 26 in Paderborn consists of a single basement parking level and an open parking deck, with approximately 99 parking spaces over about 2,200 m². LPI Ingenieurgesellschaft mbH prepared the rehabilitation and CP design. Peter Presch GmbH carried out the concrete rehabilitation and commissioned CATÓDICA GmbH to execute the CP works.

The rehabilitation followed a series of investigations in 2017, 2021 and 2024. Elevated chloride contents were found on the horizontal upper surfaces of column socket foundations and a wall foundation. The investigated vertical faces in contact with soil were less affected. Rust staining and run off marks were also visible on a beam. An exploratory opening showed no significant reinforcement damage at that position, although the near surface concrete contained elevated chlorides [2].



Fig. 1. *Paderborn before rehabilitation: rust staining and run off marks on a beam [2].*

3.2 In situ investigations

CATÓDICA carried out electrical continuity measurements and potential mapping, complemented by chloride testing by LPI. The measurements showed that reinforcement was connected within individual members, while connections between columns, walls and beams could not be assumed. The cathode connections were arranged accordingly. Cover measurements, potential maps and chloride results were brought together to define the protected regions and locate the monitoring electrodes.

The CP installation was divided into six zones covering column bases, column socket foundations, wall bases, wall strip foundations, beams and the slab soffit. These zones extend over approximately 21, 13, 22, 3, 29 and 43 m² of concrete surface, respectively, giving a total protected surface of about 131 m².

3.3 CP design

Discrete durAnode4 anodes were selected to suit the different members and installation depths. Active anode lengths of 100, 200 and 300 mm allow current to be introduced at the required positions within the concrete. The design current density was set at 15 mA/m² of steel surface for wall and column bases and 12.5 mA/m² for the other member groups in the component design schedule.

A typical column base is fitted with four 200 mm and two 300 mm anodes. Additional 200 mm anodes protect the socket foundation; the standard arrangement uses 14 anodes per socket. The number and position of anodes are adapted locally to the foundation geometry and available installation space, as shown in the column and foundation details.

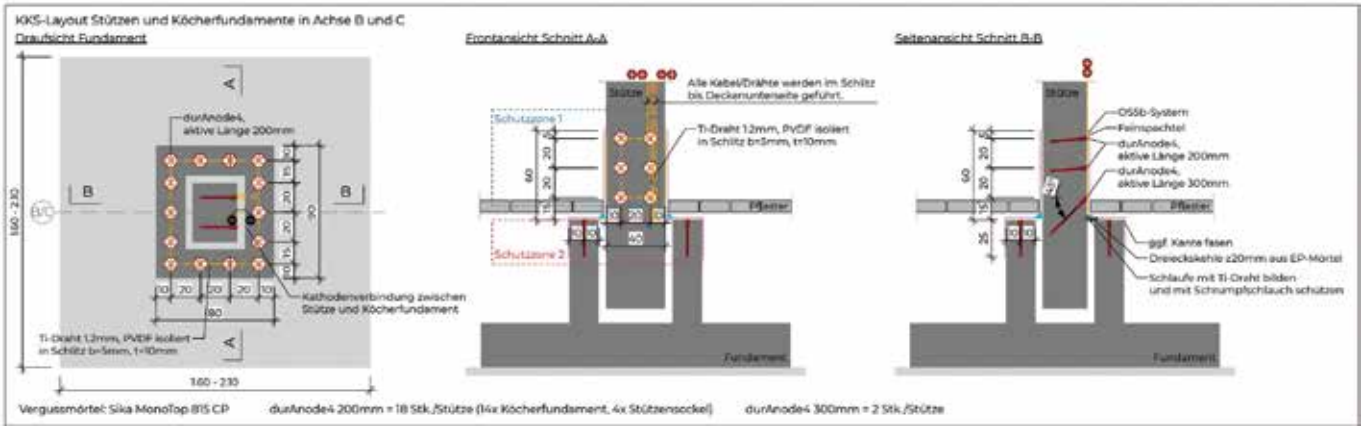


Fig. 2. *Paderborn: anode arrangement at a column base and socket foundation, with separate protection regions.*

3.4 Installation

The anodes were placed in prepared holes and embedded in Sika MonoTop 815 CP. Wall bases received 100 mm anodes and the wall strip foundations 200 mm anodes. Along beams and slab soffits, 100 mm anodes were installed at approximately 250 mm centres.



Fig. 3. *Paderborn: installation of discrete anodes at a column base and socket foundation.*

Permanent cathode connections were made to the reinforcement, together with separate current free connections for potential measurements. Mn/MnO_2 reference electrodes were embedded at the selected monitoring positions. Plastic cable ducts along the perimeter and beams carry the wiring and provide access to the distributed controllers. Local measurement modules communicate with the control unit, and an LTE connection allows the installation to be monitored remotely.

3.5 Commissioning

Anode embedment was completed in October 2025, and the six protection zones were commissioned on 1 December 2025. A driving voltage of 1.6 V was applied initially. Measurements were logged every 60 seconds during commissioning and hourly afterwards, with an instant off sampling delay of 100 ms. The reinforcement potentials shifted in the negative direction as the zones were energised.

During the first depolarisation test on 3 April 2026, the 100 mV criterion was achieved at 23 of the 26 reference electrodes. The other three locations required individual evaluation against the applicable protection criteria and, where necessary, adjustment of the operating settings. Continued inspection and monitoring provide the basis for this fine tuning.

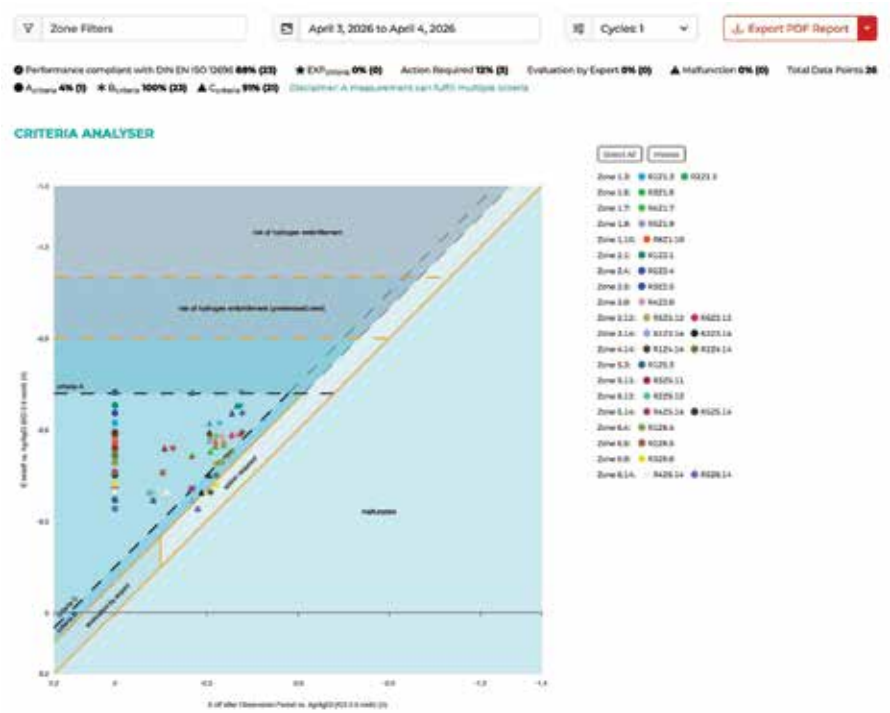


Fig. 4. *Paderborn: depolarisation test of 3 April 2026, with the 100 mV criterion achieved at 23 of 26 monitored locations.*

4 NRW BANK UNDERGROUND CAR PARK IN MÜNSTER

4.1 Project description and condition

The NRW Bank car park at Johanniterstraße 3 in Münster has two basement parking levels and 64 parking spaces. The approximately 35 year old structure is accessed by a single lane ramp leading to the first basement level. Roxeler Ingenieurgesellschaft developed the rehabilitation and CP concept. CSE Construction GmbH carried out the concrete works, and CATÓDICA installed the CP system.

Increased chloride ingress had affected the durability of the reinforced concrete. Cracks and local deterioration were visible in the floor finish, and the transitions at wall and column bases formed vulnerable parts of the structure. The rehabilitation therefore combined concrete repairs with cathodic protection of the floors, wall and column bases and ramp.



Fig. 5. *NRW Bank before rehabilitation: cracking and local deterioration at a floor transition near a wall.*

4.2 In situ investigations

The in situ work covered electrical continuity, concrete cover, potential mapping and concrete resistivity. Both basement levels were surveyed, with cover measurements taken on 14–15 October and 30 October 2025. The results were used to locate the anodes and monitoring points and to identify areas where the irregular concrete surface required levelling or additional cover before installation.

As reinforcement drawings were unavailable, the steel surface area was established from the tender information and standard details, supported by sample measurements on site. The design used 1.50 m² of steel surface per m² of floor and 1.60 m² of steel surface per m² of wall or column base. These values formed the basis for calculating the protective current demand.

4.3 CP design

The installation was divided into twenty protection zones serving the floors, wall bases, column bases and ramp across the two basement levels. Some wall zones were subdivided into several anode areas within the same controlled zone. A design current density of 15 mA/m² of steel was adopted. The floors were fitted with 20 mm HISEO ribbon mesh anodes at 250 mm centres. With an anode design output of 5.8 mA/m, this arrangement supplies the calculated floor demand of 22.5 mA per m² of concrete.

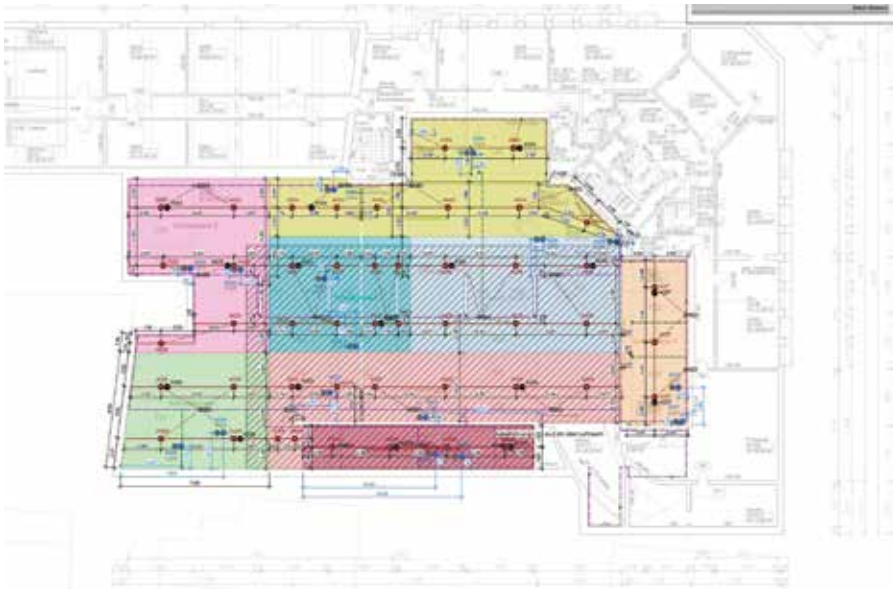


Fig. 6. *NRW Bank: anode layout and protection zones on the first basement floor.*

Wall and column bases were protected to a height of 0.50 m. Four 10 mm titanium ribbon anodes were arranged at approximately 130 mm vertical spacing, starting 50 mm above floor level. At the junction with the floor, the anodes were integrated into the repair and embedment layers. Additional cover was provided where required by the condition of the substrate.

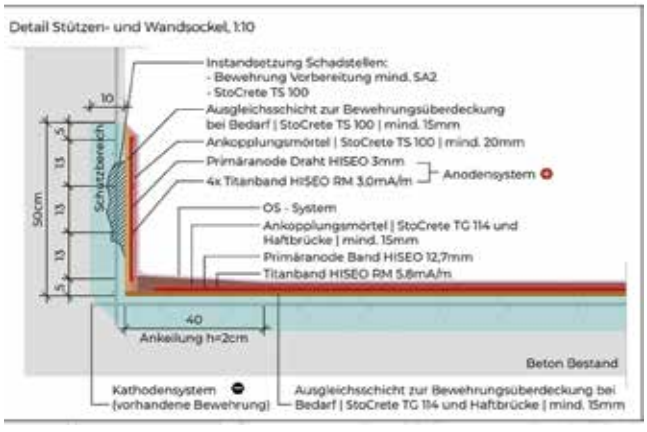


Fig. 7. *NRW Bank: construction detail at the junction between the floor and a wall or column base.*

4.4 Installation

On the floors, the ribbon anodes were embedded in StoCrete TG 114 with a TH 110 bonding bridge. StoCrete TS 100 was used at wall and column bases. Connections to the reinforcement formed the cathode circuit, with separate connections for potential measurements. Mn/MnO_2 reference electrodes were embedded at the monitoring positions.



Fig. 8. *NRW Bank: ribbon anodes on a column base and the surrounding floor before embedment.*

The controllers and local measurement modules were connected through accessible cable ducts. An ACTIVELINK unit provides central control and data acquisition, while an LTE modem enables remote communication. This arrangement keeps the embedded anodes and electrodes connected to electronics that remain accessible for inspection and maintenance.

4.5 Commissioning

Following completion of anode embedment in November 2025, the twenty protection zones were commissioned on 18 December 2025. Initial driving voltages of 1.3 or 1.5 V were applied. Measurements were taken every 60 seconds during commissioning and hourly afterwards, with a 100 ms instant off delay.

The first depolarisation test took place on 30 January 2026. The 100 mV criterion was achieved at 39 of the 40 reference electrodes. The monitoring system allows the potential trends to be followed and the operating settings to be adjusted during subsequent inspection and fine tuning.

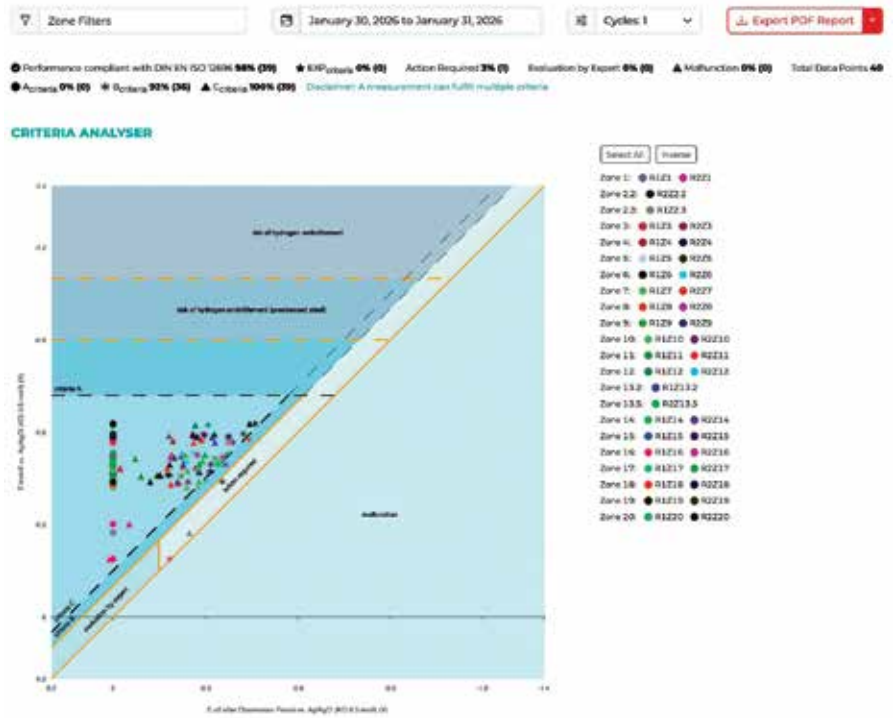


Fig. 9. *NRW Bank: depolarisation test of 30 January 2026, with the 100 mV criterion achieved at 39 of 40 monitored locations.*

5 SCHARNHORSTSTRASSE UNDERGROUND CAR PARK IN MÜNSTER

5.1 Project description and condition

The underground car park at Scharnhorststraße 44–48 in Münster has a single parking level covering approximately 6,100 m². A two lane ramp provides access at the south western side. Moisture exposure at unprotected wall and column bases, together with chloride ingress through the upper floor surface and around cracks, made rehabilitation necessary. Roxeler Ingenieurgesellschaft developed the repair concept, CSE Construction GmbH carried out the concrete works and CATÓDICA installed the CP system.



Fig. 10. *Scharnhorststraße before rehabilitation: wet floor conditions during the site visit on 15 February 2024.*

5.2 In situ investigations

Continuity measurements, cover surveys, potential mapping and concrete resistivity assessment formed the basis of the CP design. Floors and vertical members were investigated separately to account for their different geometry and exposure. As reinforcement drawings were unavailable, the steel surface area was established from the tender information and standard details and checked by sample measurements on site.

The floor design used a steel surface ratio of 0.86 m² per m² of concrete. Wall and column bases were designed with a ratio of 1.60 m²/m². The resulting current demand allowed a narrower ribbon anode to be used on the floor than at the NRW Bank project.

5.3 CP design

Forty three protection zones were arranged across the floors and the bases of walls, columns and fire door walls. The design scope comprised approximately 6,141 m² of floor surface, 316 m² of wall bases and 121 m² of column bases. Separate zones allow the current supply to be adapted to these different parts of the structure.

The floor system uses 10 mm HISEO titanium ribbon anodes at 230 mm centres. A design current density of 15 mA/m² of steel gives a floor current demand of 12.9 mA per m² of concrete. At wall and column bases, four 10 mm ribbons provide protection to a height of 0.50 m. Discrete durAnode4 anodes with an active length of 100 mm were selected for the fire door wall bases to accommodate the local construction detail.



Fig. 11. *Scharnhorststraße: layout of the distributed CP installation and protection zones.*

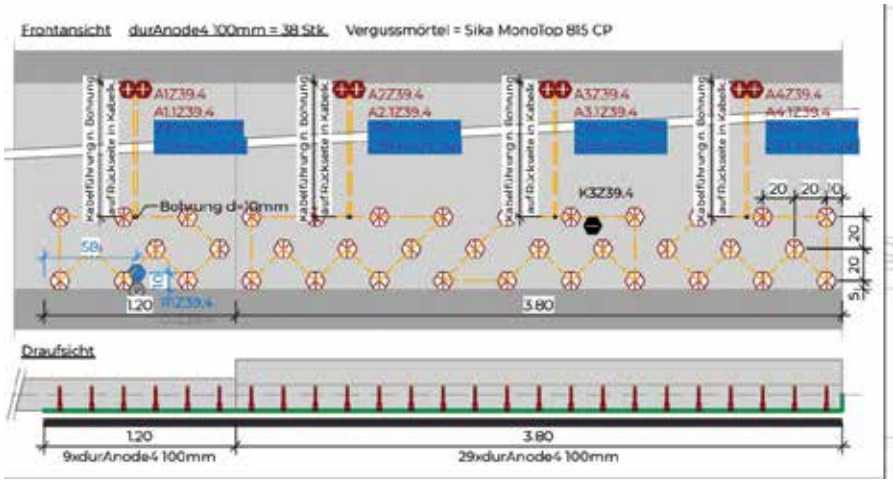


Fig. 12. *Scharnhorststraße: discrete anodes, connections and reference electrodes at a fire door wall base.*

5.4 Installation

The floor ribbons were embedded in StoCrete TG 114/118 with a TH 110 bonding bridge, which also formed part of the reprofiling work. StoCrete TS 100 was used at wall and column bases, and Sika MonoTop 815 CP around the discrete anodes. The ribbons on vertical members were arranged at approximately 130 mm spacing, starting 50 mm above the floor. Permanent cathode connections, separate current free measurement connections and embedded Mn/MnO_2 electrodes completed the monitoring arrangement.

Cable ducts follow the column rows and distribute the connections to the floors and vertical members. The controllers remain accessible, while the measurement modules are located close to the reference electrodes. ACTIVELINK and APWRLINK units provide control, communication and power distribution, with an LTE modem installed at the ramp. Clear identification of the zones, electrodes and channels supports inspection and maintenance across the large installation.



Fig. 13. *Scharnhorststraße: floor ribbon anodes before the cementitious embedment layer.*

5.5 Commissioning

The 43 protection zones were commissioned on 10 December 2025. Initial driving voltages ranged from 1.2 to 1.6 V. Measurements were logged every 60 seconds during commissioning and hourly afterwards, with an instant off delay of 100 ms. The reinforcement potentials shifted negatively as the protective current was applied.

The first depolarisation test was carried out on 26 December 2025. The 100 mV criterion was achieved at 111 of the 130 reference electrodes. The remaining nineteen locations required further assessment of the potential response, measurement validity and applicable protection criteria, together with adjustment of the operating settings where necessary.

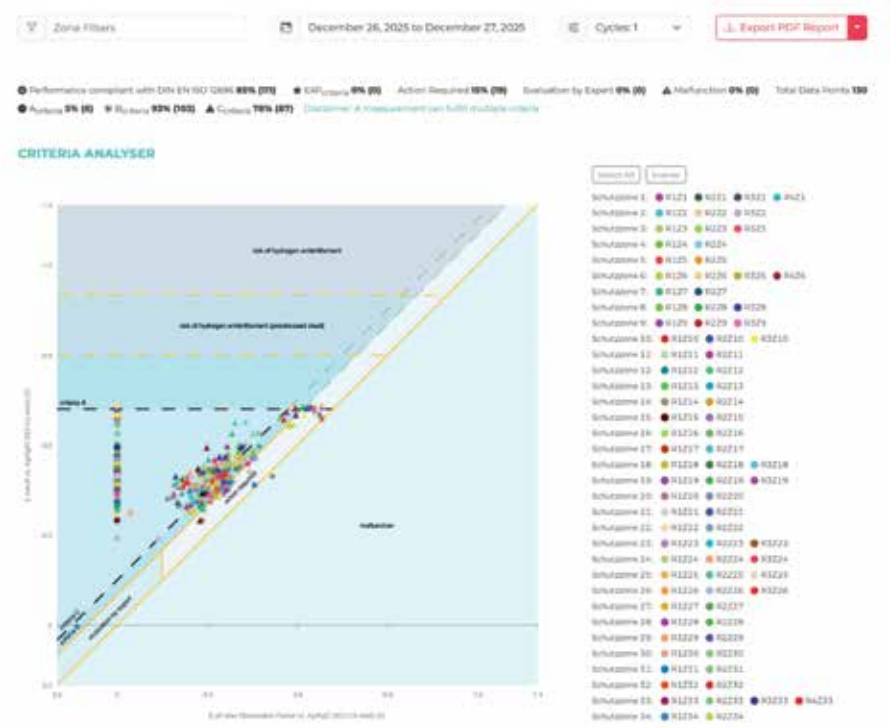


Fig. 14. *Scharnhorststraße: depolarisation test of 26 December 2025, with the 100 mV criterion achieved at 111 of 130 monitored locations.*

6 PRACTICAL EXPERIENCE

6.1 Anode selection and installation

Each structure called for a different installation approach. At Paderborn, discrete anodes could be placed within individual column bases, foundations, beams and soffits. The extensive floors and base regions in Münster were suited to ribbon anodes embedded in cementitious layers. At Scharnhorststraße, combining ribbon and discrete anodes allowed the system to continue through the fire door wall details. In each case, the anode arrangement followed the geometry of the existing members and the current needed by their reinforcement.

The two Münster projects also show the influence of reinforcement quantity. Both were designed with 15 mA/m² of steel, but the floor steel surface ratios of 1.50 and 0.86 m²/m² led to different current demands. The NRW Bank floor therefore received 20 mm ribbons at 250 mm centres, while 10 mm ribbons at 230 mm centres were used at Schar-

nhorststraße. Matching ribbon output and spacing to the steel surface area provides the required current distribution without relying on the floor area alone.

6.2 Monitoring and operation

The embedded reference electrodes make it possible to follow the response of the reinforcement after energisation and during depolarisation tests. The first tests achieved the selected criterion at 23 of 26 monitored positions in Paderborn, 39 of 40 at NRW Bank and 111 of 130 at Scharnhorststraße. Each test provided a starting point for assessing individual locations and fine tuning the installation. As the tests took place at different intervals after energisation, the results describe the initial response of each system rather than a comparison of the anode types.

Routine operation combines remote monitoring with site inspections and periodic performance checks. Where the 100 mV criterion is not reached, the potential history and measurement conditions are examined and the alternative criteria in ISO 12696 are considered. Any change in operating voltage is assessed together with the response at the other monitored positions in the zone. Accessible controllers, clearly identified wiring and reliable measurement channels make these tasks easier throughout the operating life of the installation [1].

6.3 Remote monitoring and control

With embedded sensors, cathodic protection also provides a window into the structure. Steel potentials, protective currents and operating voltages make the electrochemical response of the reinforcement visible over time. Their trends help specialists recognise changes, check the protection performance and plan targeted maintenance. The installation therefore combines corrosion protection with an ongoing view of the reinforcement's condition [1, 6].

ACTIVECONTROL SYSTEMS brings together measurement hardware, local controllers, software and the APORTAL cloud platform. Data from the reference electrodes and measurement modules can be reviewed remotely, while authorised specialists can assess depolarisation tests and adjust the protection settings. Cloud access, trend analysis and alarm functions support timely intervention and reduce the need for routine visits solely to collect measurements [6]. In this way, the CP installation becomes part of an intelligent, connected structure, helping owners maintain their property according to its measured condition.

7 CONCLUSIONS

The three projects show how cathodic protection can be adapted to existing reinforced concrete structures, combining local repairs with controlled protection of the reinforcement. Its main advantage is the opportunity to preserve serviceable concrete while addressing the corrosion process.

In conventional repair by concrete replacement, covered by EN 1504-9, Method 7.2, chloride-contaminated concrete is removed to the extent established by the condition assessment and repair design, and replaced with suitable mortar or concrete [3]. Widespread contamination can lead to extensive breakout, temporary structural propping and lengthy reinstatement and curing stages [5]. For car parks and occupied properties, this can mean prolonged closures, disruption to users and loss of parking or rental revenue.

Cathodic protection, recognised under Principle 10 of EN 1504-9, allows sound chloride-contaminated concrete to remain in place while the reinforcement is protected [1, 3]. Necessary repairs to damaged concrete and structurally deficient members are still carried out. Reducing the extent of concrete removal can preserve the original structure, limit temporary support requirements and help shorten closures, reducing the interruption to the owner's use of the property [5].

Retaining concrete also reduces demolition waste and the demand for replacement materials, with potential savings in material-related CO_2 emissions. Paul Steinmetz's comparative life cycle assessment provides a positive environmental evaluation of cathodic protection. For the investigated underground car park, the 50-year assessment of production and use gave a global warming potential of 105 t CO_2-equivalents for CP compared with 238 t for concrete replacement, a reduction of approximately 56 %. Electricity consumption contributed only a small share of the CP system's emissions [4]. These case study results demonstrate the substantial potential for reducing environmental impacts through cathodic protection. Where the structure is suitable and continued monitoring and maintenance are provided, cathodic protection can in many cases offer the best overall rehabilitation option for the structure and its owners, balancing material preservation, operational continuity, whole life cost and environmental impact.

8 REFERENCES

[1] DIN EN ISO 12696:2022-08. Cathodic protection of steel in concrete. German version EN ISO 12696:2022.

[2] LPI Ingenieurgesellschaft mbH. TG AfA Paderborn. Ergänzende Bauwerksdiagnostik. Report I2109102-02, 2024; and associated photographic condition documentation.

[3] DIN EN 1504-9:2008-11. Products and systems for the protection and repair of concrete structures. Part 9: General principles for the use of products and systems. German version EN 1504-9:2008.

[4] Steinmetz, P. (2025). Vergleichende Ökobilanzierung zwischen Instandsetzung mittels Betonaustausch und Instandsetzung mittels Kathodischen Korrosionsschutzes. Masterarbeit, Technische Universität München; Zusammenfassung in fkks Mitteilungen 1/2025, pp. 1–5. https://fkks.de/1-2025.pdf

[5] Ducasse-Lapeyrusse, J., et al. (2023). Assessment of the Impressed Current Cathodic Protection system after 4 years operation: Case study of the Saint-Cloud Viaduct (France). Case Studies in Construction Materials, 18, e02023. doi:10.1016/j.cscm.2023.e02023.

[6] ACTIVECONTROL SYSTEMS. Technologie. https://activecontrol-systems.com/technologie/ (accessed 22 October 2026).